Combinatory effects of cisplatin and 17AAG treatment in DLBCL

Master of Science Thesis

Medicine with Industrial Specialization

Biomedicine

Author:

Hulda Haraldsdóttir

AALBORG UNIVERSITET

AALBORG UNIVERSITY HOSPITAL

AALBORG UNIVERSITET

Project title: Combinatory effects of cisplatin and 17AAG treatment in DLBCL

Project period: 1st of September 2020 - 1st of May 2022

Group number: 9026

ECTS: 60

Supervisor:

Karen Dybkær, Professor
Department of Clinical Medicine, Aalborg University/Department of Hematology, Aalborg University Hospital

Co-Supervisors:

Allan Stensballe, Associate Professor

Hanne Due, Postdoc

Linnéa Schmidt, Postdoc

Issa Ismail Issa, PhD fellow

Christopher Aboo, PhD fellow

Author:

Hulda Haraldsdóttir

_____

Hulda Haraldsdóttir

Master of Science in Medicine with Industrial Specialization,

Master of Science Thesis, 9th and 10th semester.

Total page count: 70

Acknowledgements

This master thesis was developed during the last two semesters of my master's in Medicine with Industrial Specialization, Biomedicine, at Department of Health Science and Technology, at Aalborg University. The experimental work contributing to this thesis' results was conducted from September 2020 to December 2020, followed by a one-year maternity leave, and starting again from January 2022 and to May 2022. The experiments were conducted in the Laboratory of the Department of Hematology at Aalborg University Hospital and in the Laboratory of the Department of Health Science and Technology at Aalborg University.

I would like to start by thanking my main supervisor, professor Karen Dybkær for extraordinary leadership of the Laboratory Group at the Department of Hematology at Aalborg University which I luckily have been a part of through the course of my master's along with my co-supervisors, Hanne Due, Issa Ismail Issa and Linnéa Schmidt. They have offered outstanding guidance, helpful advices, and admirable dedication.

I want to thank my co-supervisors at the Department of Health and Science and Technology at Aalborg University, Allan Stensballe and Christopher Aboo for professional guidance and helpful discussions.

A special thanks to laboratory technician Helle Høholt for guidance in the laboratory and office companionship. Additional thanks to Alexander Schmitz for help with flow cytometry.

I am very thankful for my loving and supportive family and friends. Last but not least, heartfelt gratitude to Martin for immeasurable loyalty, understanding and motivation. Thank you for giving me and our son the greatest support and comfort.

Abbreviations

17AAG	17-allylamino-17-demethoxy-geldanamycin
53BP1	P53-binding protein 1
ABC	Activated B-cell-like
ANOVA	Analysis of variance
AP site	Abasic site
AUC	Area under the curve
BCR	B-cell antigen receptor
BER	Base excision repair
CSR	Class switch recombination
DDR	DNA damage repair
DLBCL	Diffuse large B-cell lymphoma
DMSO	Dimethyl sulfoxide
DNA-PKcs	DNA-dependent protein kinase catalytic subunit
DSB	Double-strand break
dsDNA	Double stranded DNA
DSMZ	German collection of microorganisms and cell cultures GmbH
FBS	Fetal bovine serum
FSC	Forward scatter
γH2AX	Phosphorylated H2AX
GC	Germinal center
GCB	Germinal Center B-cell-like
GEP	Gene expression profiling
GGR	Global genome repair
HEK cells	Human Embryonic Kidney 293 cells
HR	Homologous recombination
HSP90	Heat shock protein 90
IDLs	Insertion or deletion loops
Igs	Immunoglobulins
IPI	International Prognostic Index
LC-MS/MS	Liquid chromatography tandem mass spectrometry
LDH	Lactate dehydrogenase
MMR	Mismatch repair
NHEJ	Non-homologous end joining
NER	Nucleotide excision repair
NHL	Non-Hodgkin lymphoma
PBS	Phosphate-buffered saline
PCA	Principal component analysis
PCR	Polymerase chain reaction
PI	Propidium Iodide
R-CHOP	Rituximab (R), cyclophosphamide (C), doxorubicin (H), vincristine (O) and prednisolone (P)
R-DHAP	Rituximab (R), dexamethasone (DH), cytarabine (A), cisplatin (P)
R-GDP	Rituximab (R), gemcitabine (G), dexamethasone (D), cisplatin (P)
R-ICE	Rituximab (R), ifosfamide (I), carboplatin (C), etoposide phosphate (E)
rrDLBCL	Relapse or refractory DLBCL
SHM	Somatic hypermutation
SSC	Side scatter
TCR	Transcription-coupled repair (TCR)
TEAB	Triethylammonium bicarbonate
VDJ	Variable (V), diversity (D), and joining (J) Ig-gene segments

Table of contents

Abstract

Background: Cisplatin is an efficient antitumor agent used as salvage treatment for DLBCL patients that have relapsed or become refractory to their first-line treatment (rrDLBCL). However, approximately 70% of rrDLBCL patients will again experience relapse of their disease after salvage treatment caused by various factors, such as resistance towards the drugs, including cisplatin. This leaves the patients with few therapeutical options and poor prognosis. Cisplatin resistance has been linked with overexpression of components of the DNA damage response (DDR), thus, inhibiting DDR during cisplatin exposure could plausibly improve cisplatin efficacy and response. 17AAG is a potent Hsp90 inhibitor that through binding to the Hsp90 complex leads to degradation of its clients including components of the DDR and have therefore been considered as an add-on drug to cisplatin treatment.

Hypothesis: We hypothesize that 17AAG can sensitize DLBCL cells to cisplatin, whereby cisplatin resistance can be overcome.

Methods: Two DLBCL cell lines, RIVA and SU-DHL-5, were investigated after treatment with cisplatin and 17AAG as single drugs and in combination, along with vehicle controls for effect on DNA damage, cell cycle distribution and apoptosis activity with flow cytometry. Additionally, cell viability was determined with cell counting assay and differential DDR protein expressions were investigated with quantitative proteomic analysis in the treated DLBCL cells through time.

Results: Synergistic effects of combining 17AAG with cisplatin was observed in RIVA characterized by increased DNA damage, disturbed cell cycle distribution, increased apoptosis and decreased cell viability. However, synergistic effect in SU-DHL-5 was not observed, suggesting a cell line specific combinatory effects in resistant DLBCL cells, such as RIVA. Furthermore, tendencies of decreasing effect on expression of the DDR proteins MSH2 and MSH6 was observed for both cell lines after treatment with 17AAG, implying that the synergistic effects of cisplatin and 17AAG could at least partly be based on 17AAG's inhibitory effect on DDR proteins.

Conclusion: This thesis has discovered that 17AAG sensitizes cisplatin resistant DLBCL cells to cisplatin. Thus, constituting a potential treatment strategy to overcome cisplatin resistance.

1. Introduction

1.1 B-cell development

B-cells are a type of lymphocyte and key players in the humoral adaptive immunity by producing antibodies, also known as immunoglobulins (Igs) which identify, neutralize and clear antigen expressing pathogens [1]. The Igs produced by the B-cells are either secreted or expressed as a part of the surface transmembrane protein named the B-cell antigen receptor (BCR), depending on the differentiation step of the B-cell. Both forms of Igs can bind to antigens and in that way initiate the humoral immune response [2]. The BCR contains two heavy chain and two light chain Ig polypeptides that are linked by disulfide bridges (Figure 1A) [3]. The B-cells' ability to bind a variety of antigens lies in the diversity and specificity of the BCR which is unique for each B-cell [2]. The BCR diversity is generated during early developmental stages of B-cells by rearrangement of the variable (V), diversity (D), and joining (J) Ig-gene segments, that constitute BCR's heavy and light chains (Figure 1B) [4]. B-cell development starts in the bone marrow where pluripotent hematopoietic stem cells differentiate into precursor B-cells in the developmental stages called early and late pro-B-cells, pre-B-cells, immature B-cells and naïve B-cells (Figure 1C) [5]. At the early pro-B-cell stage, the first rearrangement of Ig-gene segments of the heavy chain is performed between the D and J segments. If the rearrangement of D and J segments is successful, the cell is considered as a late pro-B-cell whereafter the D and J segment is recombined with a V segment. The generated functional VDJ segment will be spliced to the constant Igμ gene, generating the heavy chain that will be expressed along with surrogate light chain proteins as a pre BCR on a pre-B-cell [6,7]. If the pre BCR can bind to ligands in the bone marrow microenvironment it is rescued from apoptosis by positive selection confirming a functional Igμ chain. This induces signaling activation of proliferation and rearrangement of the V and J segments of the light chain to generate a complete BCR. An immature B-cell is characterized by a complete BCR with functional heavy and light chains and the immature B-cell will go through a negative selection to eliminate cells with autoreactive BCRs where the remnant cells will be considered mature naïve B-lymphocytes that can leave the bone marrow to the blood vessels and enter secondary lymphoid tissue for activation.

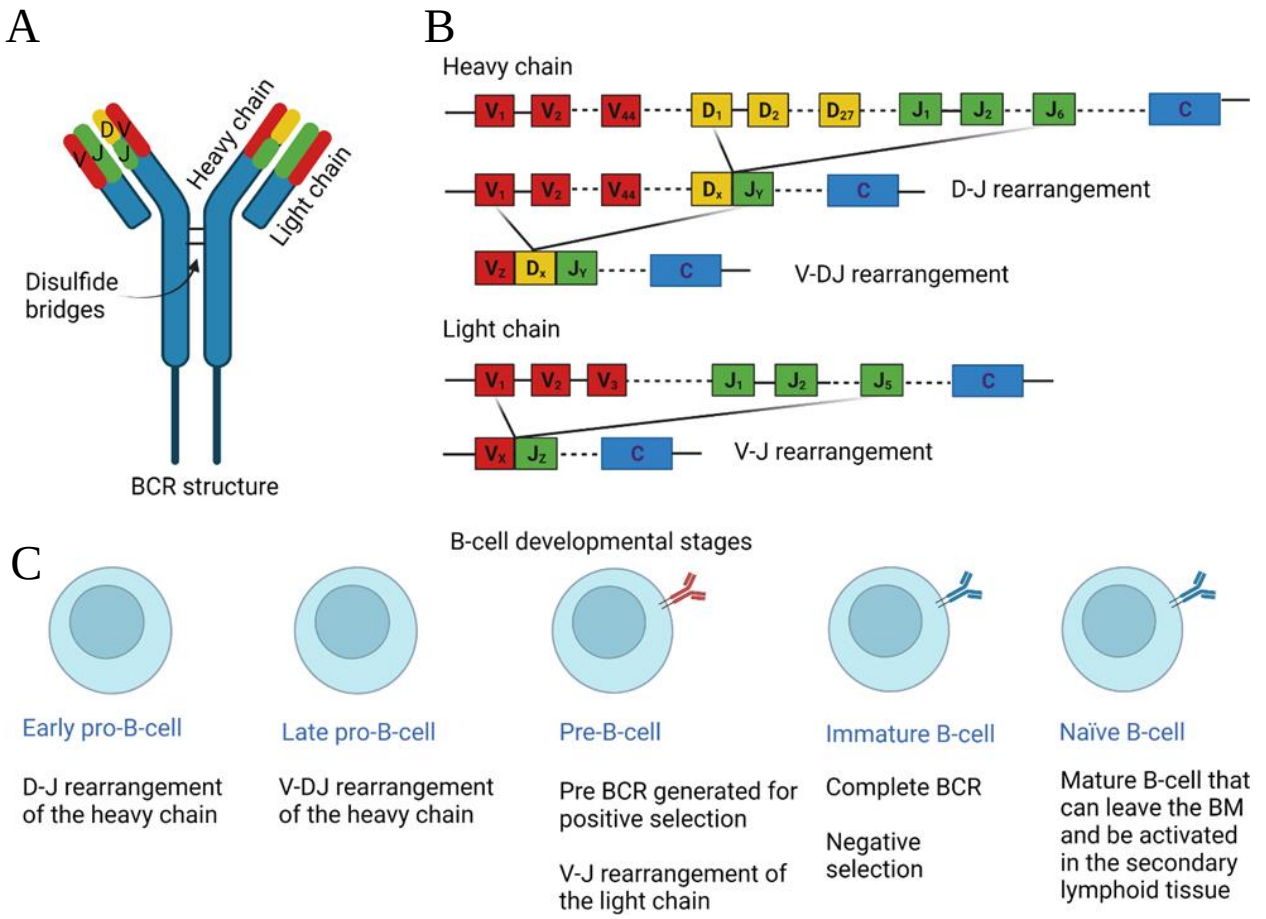

Figure 1: B-cell development and B-cell receptor (BCR) diversity process. A: The BCR is composed of two heavy chains and two light chains, constituting various Ig-gene segments (Variable (V), diversity (D) and joining (J) segments). The heavy and light chains are linked by disulfide bridges. B: The VDJ rearrangement process when heavy and light chains are generated under B-cell development. C: The B-cell developmental stages are early pro-B-cell, late pro-B-cell, pre-B-cell, immature B-cell and naïve B-cell.

If the naïve B-lymphocytes encounter an antigen in the secondary lymphoid tissue, they become activated with help from antigen-specific T-cells, priming the germinal center (GC) that consists of a dark and a light zone (Figure 2). Upon activation, the B-cells differentiate into centroblasts that proliferate at high speed and generate the dark zone of the GC. Simultaneous to the high level of proliferation, the centroblasts undergo somatic hypermutation (SHM) of the V segments of the BCR [8]. SHM is initiated by the enzyme Activation-Induced Cytidine Deaminase that introduces mutations to the V-segment by deaminating the DNA nucleobase cytosine into deoxy-uracil (U). Normally, this mutation can be sufficiently repaired by the DNA damage repair (DDR) system of the cells. However, the B-cells exhibit higher tolerance for mutations induced during SHM, restricting the DDR to respond as the generated mutations lead to variations in the BCR affinity [9].

Subsequently, the centroblasts become centrocytes with hypermutated BCR expression and migrate from the dark zone and to the light zone of the GC [8]. Here, the centrocytes reencounter the antigen where only the centrocytes expressing BCRs with improved affinity to the antigen will survive whereas centrocytes that have developed lower BCR affinity will undergo apoptosis - a process called affinity maturation [8,9]. The centrocytes can go through this process multiple times by recycling between the dark and the light zone. Following affinity maturation, the centrocytes undergo class switch recombination (CSR) enabling a switch of the constant Ig gene that encodes the isotype of the cell resulting in change of which antibodies are produced (IgM, IgG, IgA, IgE or IgD) [9,10]. Ultimately, the B-cells can leave the GC and progress and mature into antibody-secreting plasma cells or memory B-cells (Figure 2) [7].

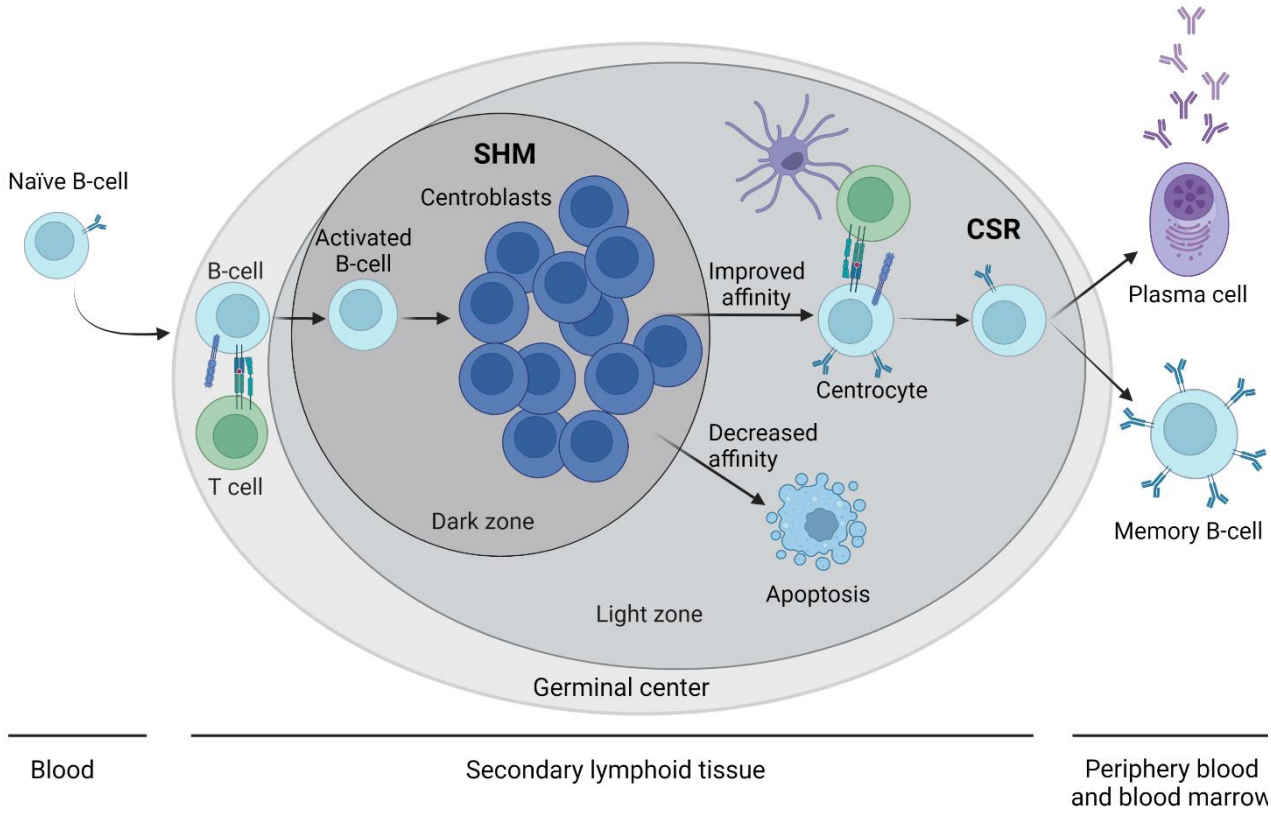

Figure 2: Upon activation of a B-cell, the germinal center is generated where the B-cell differentiate into centroblasts that proliferate at high speed and undergo somatic hypermutations (SHM) resulting in centrocytes with various antigen affinity. The centrocytes travel from the dark zone and to the light zone where only the ones with improved affinity bind to an antigen and survive. The remainder centrocytes undergo class switch recombination (CSR) and ultimately differentiate into antibody-secreting plasma cell or memory B-cell.

Accordingly, the development of antigen-specific B-cells involves double stranded DNA breaks with three rearrangements of the Ig-gene segments in the bone marrow in addition to SHM and CSR in the GC, exposing B-cells to high levels of DNA damage. In addition, B-cells have high DNA damage tolerance with restricted DDR response where proliferation is maintained despite occurred mutations [9]. This increases the risk of malignant transformation where the tolerated genomic instability of the B-cells can lead to retained oncogenic mutations which can result in lymphomagenesis [11,12].

1.2 Lymphomas

Lymphomas are a group of hematological malignancies arising from lymphocytes that constitute important cells of the immune system, such as B-cells, T-cells and natural killer cells [13,14]. Lymphomas are characterized by uncontrolled growth of cells that can invade surrounding tissues and organs [15]. The cancer cells acquire these capabilities by a series of genetic mutations and epigenetic changes that enable the cancer cells to thrive [16]. These capabilities have been described as the hallmarks of cancer [11], and include sustained proliferative signaling, enabled replicative immortality, resistance of cell death, evasion of growth suppressors, induced angiogenesis, and activated invasion and metastasis. Furthermore, two additional emerging hallmarks have been proposed, namely altered cellular metabolism and avoidance of immune destruction [18]. The hallmarks can be acquired by lymphocytes at various stages of their differentiation, resulting in lymphomas [14].

Lymphomas are broadly divided into two main groups termed Hodgkin lymphomas and non-Hodgkin lymphomas (NHLs), with the latter having a higher prevalence of approximately 90% [19,20]. In Denmark, approximately 1400 new cases of NHLs are registered every year [21]. A minimal number of NHL cases originates in T- and natural killer cells, whereas malignant B-cells account for 85% of the cases, of which the majority are diagnosed with diffuse large B-cell lymphoma (DLBCL) [19].

1.3 Diffuse Large B-cell Lymphoma

DLBCL is the most common type of NHL and accounts for 30-40% of NHL globally, making it the most prevalent lymphoid malignancy in adults [22]. Approximately 450 new DLBCL cases are diagnosed in Denmark every year [23]. The incidence of DLBCL is more prevalent in males and increases with age, thus, patients diagnosed are primarily elderly patients with a median age of 67 years in Denmark [24,25]. The etiology of most DLBCL cases remains unknown. Distinctions are made between cases where the tumor arises de novo, referred to as primary disease, and where the

tumor arises by progression or transformation of indolent lymphoma, referred to as secondary [24,26]. DLBCL originates from medium or large-sized B-cells with large nuclei and grow in a diffuse pattern [27]. It is an aggressive disease usually involving single or multiple lymph nodes typically located on the neck, mediastinum, or abdomen. However, extranodal sites such as the gastrointestinal tract, skin, and head are seen in 40% of cases [22,24,28]. Approximately 30% of patients display B-symptoms including fever, night sweats and weight loss, as well as symptoms related to organ involvement. The patient's blood sample can show increased serological protein biomarkers, including lactate dehydrogenase (LDH) and beta-2-microglobulin, which can help with diagnosis of DLBCL [22,24].

1.3.1 Diffuse Large B-cell Lymphoma subclassifications

DLBCL is a clinical, pathological and molecular heterogeneous disease, reflected in largely diverse patient groups with a 5-year survival rate variation of 30-80% [28]. Risk-stratification assessment of DLBCL patients have been developed with a clinical scoring system called International Prognostic Index (IPI) that is widely used in clinical practices for prognosis assessment and selection of treatment strategies [29,30]. The IPI scoring system is based on five risk factors related to pretreatment clinical characteristics where presence of each risk factor gives a score of 1. The five risk factors are: age >60 at diagnosis, elevated LDH, extranodal involvement, Ann Arbor stage III or IV (determined by tumor localization) and Eastern Cooperative Oncology Group performance status >2 (determined by the extent of symptoms). The IPI (0-5) is scored according to numbers of present IPI risk factors, and assigns the patients into one of four risk groups: low risk (score 0-1), low intermediate risk (score 2), high intermediate risk (score 3) or high risk (score 4-5) [29]. Revised versions of IPI have been developed and introduce variances of the risk factor subcategorization, however, they have not replaced the original IPI which is still used as a standard procedure in clinical practice [30–33].

Because of the molecular heterogeneous entity of the disease, numerous subclassifications of DLBCL exist based on gene expression and genetics [34–40]. The most frequently used classification system is based on gene expression profiling (GEP) of the tumor and divides DLBCL into cell-of-origin subclassifications: Activated B-cell-like (ABC) and Germinal Center B-cell-like (GCB), where patients assigned to the latter show superior prognosis after treatment with standard chemotherapy [22,34,41]. A small group of cases cannot be classified as either of those subclassifications and are consequently termed unclassifiable [14]. ABC and GCB present distinct stages in the B-cell development where GCB resembles centroblasts and centrocytes found in the GC, while the ABC resembles activated B-cells in the peripheral blood [34,42]. In addition to differences in clinical

outcome, the two subclasses differ in genetic alterations and pathogenesis [34,43].

The transcriptional profile of GCB DLBCL patients resembles germinal B-cells that undergo ongoing SHM and CSR in the GC and are therefore characterized by highly mutative Ig-genes. Furthermore, mutations in genes involving histone methylation or acetylation such as gain of function of EZH2 and loss of function of EP300 are frequently detected in patients of the GCB subclassification as well as genes involved in B-cell homing pathway signaling, such as GNA12 and SIPR2 [22,39,40]. Moreover, the PI3K pathway and the JAK-STAT pathway are often mutated in GCB-DLBCL patients [22,40] (Table 1).

Mutations observed in ABC DLBCL patients include alterations related to the BCR where somatic gain of function mutation in CD79B, which in complex with CD79A generates BCR signaling, is detected in 20% of cases [39]. Moreover, constitutive activation of the apoptotic nuclear factor kappa is a hallmark of ABC-DLBCL, which is caused by mutations in the Toll-like receptor signaling pathways. More than 20% of these cases are caused by somatic gain of function mutation of the MYD88 gene (Table 1) [22,39,40,44].

Chromosomal alterations are frequent in DLBCL and translocations of BCL6 are seen in 35% of DLBCL patients with two- to three-fold higher frequencies in the ABC subclassification. Translocations of BCL6 or BCL2 in addition to translocation of MYC are considered as double-hit lymphoma and triple-hit lymphoma if all three loci are affected where both cases present a particularly aggressive DLBCL [39,40].

	ABC	***GCB***
Prognosis	Inferior prognosis	Superior prognosis
Origin	Activated B-cells	Germinal center B-cells
Frequent mutations	Activation of the B-cell receptor signaling (CD79B), Toll-like receptor signaling pathways (MYD88) and BCL6.	Highly mutative Ig-genes, genes involving histone methylation or acetylation (EZH2, EP300), genes involved in B-cell homing pathway (GNA12 and SIPR2), P13K and JAK-STAT signaling pathway.

Table 1: The main characterizations of Activated B-cell-like (ABC) and Germinal Center B-cell-like (GCB) cell-of-origin subclassifications based on gene expression profiling.

Additional subclassification methods have been developed constituting genetic subclassifications for further guidance of prognosis and treatment stratification. These include a subclassification of

DLBCL based on genetic driver alterations that by integration with consensus clustering have subdivided DLBCL into 5 distinct clusters (C1-C5) [36] as well as the subclassification system based on genetic features within DLBCL that by a LymphGen algorithm have identified seven distinct genetic subclassifications [37].

The many subclassification strategies of DLBCL emphasize the molecular and clinical heterogeneity of the disease, which results in patient groups with highly variable biology, treatment response and outcome. The common aim of the subclassification systems is to provide insight to the pathology underlying the malignancy, which can aid the management of the different DLBCL cases to improve patient outcome. Accordingly, the first-line standard treatment of DLBCL includes a combination of multiple drugs in order to take in account inter- and intra-patient heterogeneity, and thus targeting multiple pathological factors within each tumor and between tumors [41].

1.4 Treatment of Diffuse Large B-cell Lymphoma

The first-line treatment of DLBCL is the immunochemotherapy regimen R-CHOP. It has been the standard therapy for DLBCL patients for over a decade and consists of rituximab (R), cyclophosphamide (C), doxorubicin (H), vincristine (O) and prednisolone (P) [22,45]. Despite the aggressive entity of DLBCL, approximately 60-70% of DLBCL patients are cured of the disease after treatment with the R-CHOP regimen [22]. However, 30-40% of the patients treated with R-CHOP will not be cured of the disease but relapse or develop refractory disease (rrDLBCL) [41]. Currently, the only curative options for these patients are salvage platinum-containing chemotherapy regimens followed by autologous stem cell transplantation [46,47]. The salvage regimens used in Denmark are most commonly R-DHAP (rituximab, dexamethasone, cytarabine/Ara C and cisplatin), R-ICE (rituximab, ifosfamide, carboplatin and etoposide phosphate) or R-GDP (rituximab, gemcitabine, dexamethasone and cisplatin) [24,48]. The drug cisplatin is involved in two-thirds of the common salvage treatment regimens for rrDLBCLs and is also used as a first-line treatment for several other cancer types because of its documented efficiency as an antitumor agent [49,50].

1.5 Cisplatin

Cis-diamminedichloroplatinum(II) (cisplatin) was approved by the Food and Drug administration in 1978 and has since been widely used as an effective anticancer drug. Cisplatin is a small molecule composed of one platinum atom bound to two labile chloride groups and two amides [49,50]. Upon administration, cisplatin travels through the blood and enter cells by passive or facilitated diffusion

and by active transport. Numerous transporters have been linked to uptake of cisplatin, such as SLC22, CTR1 and CTR2 [49]. When cisplatin enters the cells, it undergoes an aquation process as a consequence of the low chloride concentration in the cytosol (Figure 3A). By this process, one or two chlorides are replaced with water molecules which makes cisplatin a potent electrophile enabling it to react with a variety of biomolecules in the cell, primarily the DNA, forming DNA adducts. In more details, the platinum atom of cisplatin covalently binds to the N_7-sites of purine bases resulting in 1,2- or 1,3-intrastrand crosslinks if the purines are on the same strand, and interstrand crosslinks if the purines are on opposite strands (Figure 3B) [49,50]. The inter- and intrastrand crosslinks disrupt the structure of the DNA and subsequently block transcription and initiate cell cycle arrest to repair the cisplatin-induced DNA damage [49,50]. The cytotoxic effect of cisplatin lies in the large extent of DNA damage leading to unsuccessful DNA reparation that signals for apoptosis of the cell [50]. In that way, cisplatin causes apoptosis of tumor cells through inducing extensive DNA damage that activates DNA reparation and subsequently apoptosis when the DNA damage remains unrepaired. Thus, the DDR system is an important part of the antitumor effect of cisplatin [49].

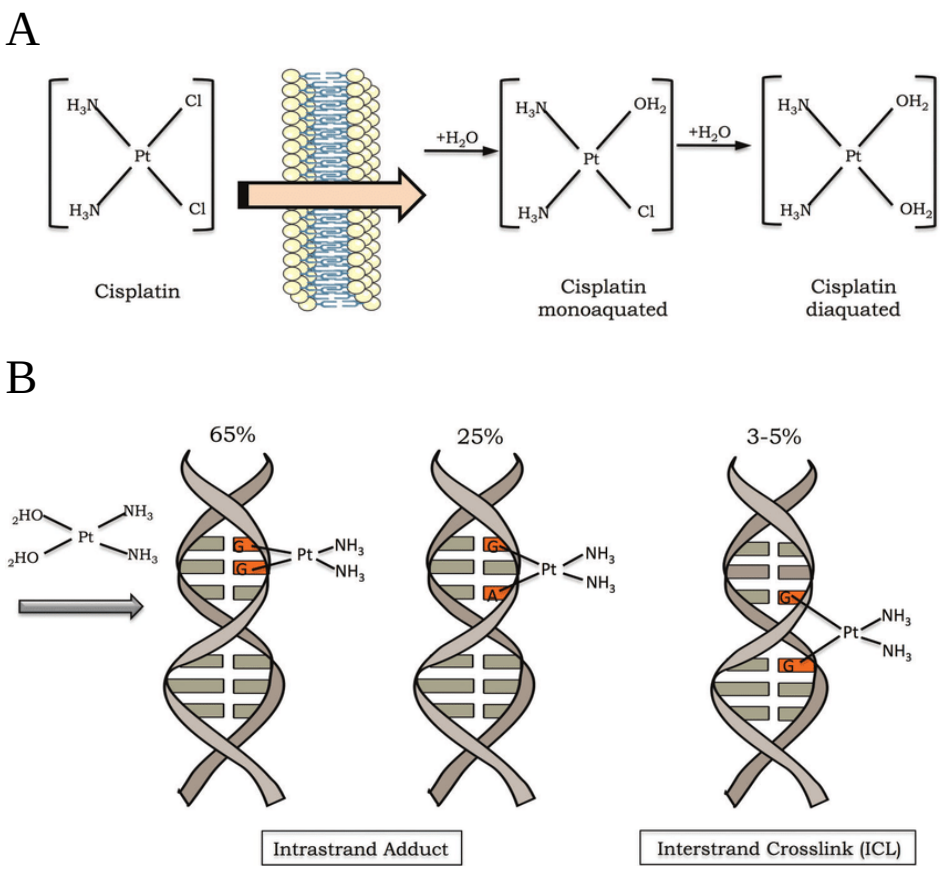

Figure 3: Cisplatin mechanisms of action. A: The aquation process when cisplatin enters the cells involving a switch of cisplatin's two chlorides with water molecules. This makes cisplatin a potent electrophile able to react with DNA of the cells. B: Cisplatin binds to the purine bases on the DNA resulting in intra- and interstrand crosslinks.
The figure is adapted from [50].

1.6 DNA damage repair

The DDR system is a cellular tool to maintain human genomic stability accomplished by a network of cellular pathways that sense, signal and repair DNA lesions. Surveillance proteins monitor DNA integrity and activate DNA repair pathways as well as cell cycle checkpoints in response to DNA damage, to prevent potential harm to the cell [51,52]. DDR is an extremely important system in B-cells because of their normal B-cell development involving rearrangement of the Ig-gene segments along with SHM and CSR that exposes B-cells to high levels of DNA damage, as stated in the first section [53]. In accordance, DLBCL is characterized by having the highest somatic mutational frequency among hematological cancers [54] and by having alteration frequencies in DDR genes in around 20% of cases [55].

The DDR constitutes five major DNA repair pathways that are active through different stages of the cell cycle, allowing cells to repair DNA damage by activation of more than 250 different DDR related genes [51,52]. The five major pathways are termed base excision repair (BER), homologous recombination (HR), non-homologous end joining (NHEJ), nucleotide excision repair (NER) and mismatch repair (MMR) (Figure 4) [56]. Of the five major DDR pathways, NER and MMR are suggested to be most involved in cisplatin's mechanism of action [50].

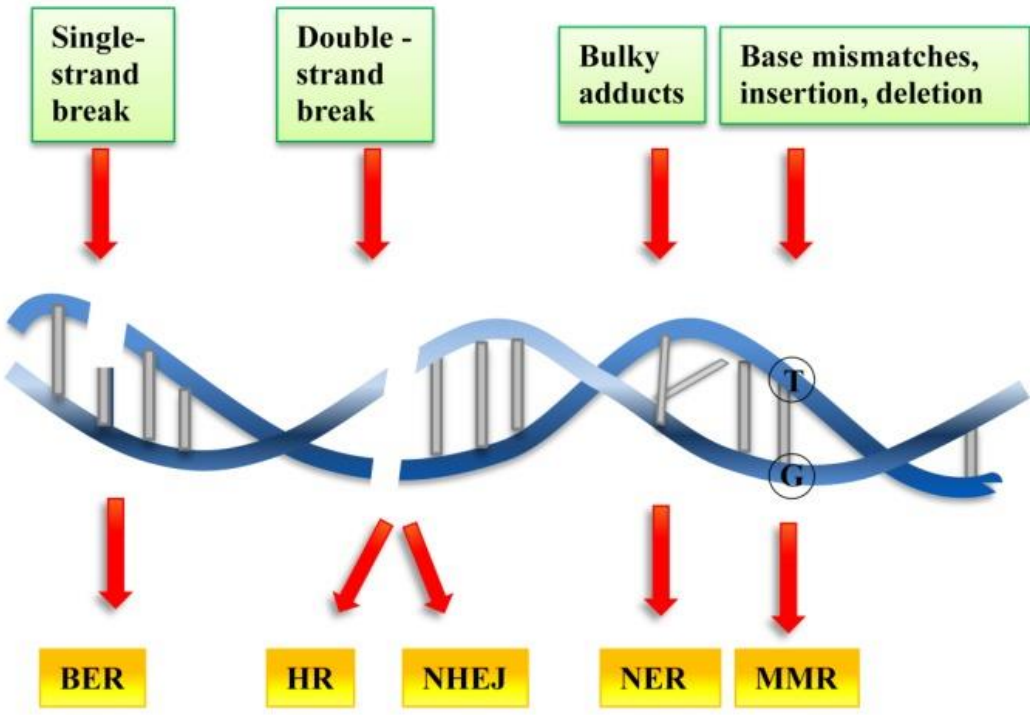

Figure 4: An overview of the five major DNA damage repair (DDR) pathways: base excision repair (BER), homologous recombination (HR), non-homologous end joining (NHEJ), nucleotide excision repair (NER) and mismatch repair (MMR). The figure is adapted from [57] and modified.

The BER pathway is responsible for repairing small base lesions and single-strand breaks that do not significantly disrupt the structure of the DNA [58,59]. These lesions result from deamination, oxidation, or methylation, caused by spontaneous decay of DNA, environmental chemicals or radiation [58]. Briefly, BER is initiated by a damage-specific DNA glycosylase that removes the damaged base resulting in an abasic (AP) site that is cleaved by AP endonuclease 1 resulting in single strand breakage which is repaired by filling the gap with deoxyribonucleoside monophosphates by the DNA polymerase and subsequently sealed with DNA ligase [59,60]. This process is regulated by various proteins, mainly XRCC1, PARP1, and PARP2 [60].

In contrast to the BER pathway, HR and NHEJ pathways repair double-strand breaks (DSBs). Many DSBs are thought to arise endogenously mainly from ionizing radiation or ROS-induced DNA damage, which is elevated in cancer cells. NHEJ repairs up to 85% of DSBs induced by ionizing radiation (e.g., in anti-cancer treatment) by ligating DSBs, however, it is suggested to be an error prone process. It is active in all cell cycle phases, primarily in G0- and G1-phases. Through the NHEJ pathway DSBs are identified with ATM and MRN complexes (including MRE11, RAD50, and NBS1 proteins) whereafter KU70 (also termed XRCC6) and KU80 (XRCC5) bind around the broken ends and recruit DNA-dependent protein kinase catalytic subunit (DNA-PKcs), forming the DNA-PK complex that generates DSBs rejoining [61,62]. In accordance, the HR pathway also utilizes the ATM and MRN complexes to identify DSBs but contrarily to NHEJ, is most active in S and G2-phases of the cell cycle. During HR, endonucleases remove one strand of the DNA duplex, located at the broken ends of a DSB to get a single strand that can be used for template for accurate resynthesis of DNA. The single strand anneals with the homologous regions in another DNA duplex and subsequently the gap, left by the damaged nucleobase, is filled. Thus, in a presence of homologous strand the DNA damage will be repaired via HR pathway and otherwise the NHEJ pathway [63].

The NER pathway repairs bulky DNA adducts generated by UV or platinum-based agents and is therefore one of the main mechanisms utilized through the cisplatin mechanism of action [50]. NER is divided into two sub-pathways termed global genome repair (GGR) and transcription-coupled repair (TCR) that differ in the process of recognizing the DNA damage whereafter they function analogously [50]. In GGR the entire genome is investigated for distortion in the DNA helix where the XPC protein in complex with RAD23B and CETN2 proteins recognize DNA lesions. Alternatively, if the lesion is not as destabilizing, it is recognized by the DNA damage binding proteins DDB1 which subsequently stimulates the binding of XPC [50,56]. The TCR sub-pathway is only activated during transcription when an RNA polymerase II is stalled by a lesion, which initiates

recruitment of the TC-NER specific protein CSA and CSB that further recruit additional proteins such as UVSSA, XAB2, and HMGN1. The CSA-CSB complex and additional components reverse translocate the RNA polymerase II resulting in an exposed lesion site [56]. After DNA damage recognition through either GGR or TCR, the TFIIH complex is recruited, and the pathway becomes shared. The TFIIH with additional XPB and XPG subunits unwind the DNA and recruit the endonuclease XPF/ERCC1. The XPG cleaves the phosphodiester chain at the 3'end and XPF/ERCC1 cleaves the 5'end resulting in dual incision. Lastly, the oligonucleotide fragment that contains the lesion is excised, leaving behind a gap that signals for repair synthesis. Here DNA polymerase Ɛ and δ, with help of the accessory proteins RFC, PCNA, and RPA, fill the gap by using the intact strand as a template, followed by ligation by LIG1 or XRCC1-LIG3 [50,56].

The MMR pathway is activated when single-strand DNA errors, including mismatched bases and insertions or deletions loops (IDLs), arise during replication. This pathway constitutes an important DDR pathway in B-cells, as it is activated during SHM and CSR in the course of normal B-cell development [56]. Furthermore, MMR identifies lesions caused by alkylating agents such as cisplatin that generates post replicative mispairing. However, MMR cannot fully repair these lesions as MMR targets the bases opposite the cisplatin DNA adduct, resulting in that MMR pathway repeatedly replaces the opposite base. This ultimately leads to DSBs which activates DNA damage signaling factors, initiating apoptosis. In that way, MMR is an important factor in the cytotoxic effect of cisplatin on cancer cells [50]. The general repair process through the MMR pathway is initiated by the MutSα (MSH2/MSH6) and the MutSβ heterodimer (MSH2/MSH3), which recognize 1-2 nucleotide IDLs and large IDLs, respectively. Next, the MutLα dimer (MLH1/MSH2) forms a complex with MutSα or MutSβ and slides up and down the DNA in an ATP-dependent manner until it encounters the replication machinery proteins PCNA and RFC which activates an exonuclease, EXO1, to cleave the DNA strand containing the nucleotide mismatch. The gap is subsequently filled by DNA polymerase Ɛ and δ, followed by ligation through LIG1 [50,56].

Besides the five major DDR pathways presented, several additional repair mechanisms exist, such as direct repair, interstrand cross-link repair, and translesion synthesis [56,62]. However, this thesis will focus on the major DDR pathways, specifically the NER and MMR pathways as they constitute the main pathways that are involved in cisplatin's molecular mechanism of action.

1.7 Resistance

Although cisplatin is defined as one of the most effective antitumor drugs for treating rrDLBCL patients, a substantial subset (70%) of patients receiving cisplatin-containing salvage regimens will experience continuous relapse of their disease leaving them with few treatment options and poor prognosis [22,46,47]. Generally, poor response of DLBCL tumors towards therapy is caused by a complex process with variety of causative elements related to the inter- and intra-heterogeneity of the disease.

There can be patient-specific causes of poor response involving host factors that affect pharmacokinetics and pharmacodynamics of the drug. The pharmacokinetic element includes absorption, distribution, metabolism, and elimination of the drug that can limit the amount of drug reaching the tumor. The pharmacodynamics of the drug presents the antitumor activity of a drug when it has reached the tumor site and is associated with drug influx/efflux, activation of the drug within the cell, alterations of expression of the drug target, adaptive pro-survival responses and evasion of cell death [64,65]. Some of these factors are included in the hallmarks of cancer, elucidating the continuous challenge of effective cancer treatment [18].

In addition to pharmacokinetics and pharmacodynamics aspects, treatment resistance constitutes another element with great impact on clinical outcome. This is the molecular background within tumor cells which is related to various epigenetic and genetic alterations as well as transcriptional and translational aberrations. The molecular drug resistance within the tumor cells can be present before or after the drug treatment. Intrinsic resistance is present before anti-cancer therapy and is mediated by pre-existing factors within the tumor which can be caused by germinal or somatic genetic mutations that decrease the effect of the therapy, resulting in primary refractory disease [64–66]. Contrarily, acquired drug resistance can be developed during therapy in initially sensitive DLBCL tumors. This can be caused by clonal expansion where mutations or epigenetic alterations in a subpopulation of cells outgrow the sensitive cells within the tumor leading to relapsed DLBCL [64,65].

Resistance to cisplatin is primarily associated with the components involved in the drug's mechanism of action. The efficacy of cisplatin is not only dependent on inducing DNA damage but also on the cell's ability to identify and respond to the damage. Thus, the DDR mechanism, responsible for the signaling pathways that regulate repair of the DNA damage and apoptosis, has high impact on how the cells respond to cisplatin [49]. As stated previously, one of the main DDR pathways activated

through cisplatin-induced DNA damage is the NER pathway which attempts to repair the intrastrand crosslink lesion. Overexpression of ERCC1 and XPA proteins involved in the NER pathways have been linked to cisplatin resistance through increased repair of the cisplatin-induced lesion [49]. Corroborating this finding, a double knockdown of XPF/ERCC1 complex in functional in vitro studies has been shown to enhance sensitivity to cisplatin [67]. Moreover, the MMR pathway is involved in cisplatin-mediated cytotoxicity as it integrates the signaling process that triggers apoptosis after recognizing cisplatin-induced DNA damage. Consequently, mutations in MSH1 or MRLH1 genes leading to MMR deficiency have been shown to have resistant effects on tumor cells [49,68,69].

Accordingly, the DDR system is associated with cisplatin response and thus using a drug targeting the DDR in combination with cisplatin has been suggested as a plausible way to overcome cisplatin resistance [49].

1.8 Targeting the DNA damage repair system

Multiple components of the DDR system have been reported to be heat shock protein 90 (Hsp90) chaperone clients meaning that Hsp90 stabilizes and activates many of the DDR proteins and in that way regulates the different DDR pathways. In that context, inhibition of Hsp90 would affect the DDR pathways and could potentially be used to sensitize cancer cells to cisplatin treatment. In addition, Hsp90 has been suggested to be a crucial facilitator of oncoproteins and is expressed in two- to ten-fold higher levels in cancer cells, compared to normal cells. Hence, Hsp90 is also a valid anti-cancer drug target on its own [70]. 17-allylamino-17-demethoxy-geldanamycin (17AAG) is a well-studied chemical inhibitor of Hsp90 that through binding to the ATP-binding region inhibits formation of the Hsp90 complex. This inhibits the chaperone function, resulting in degradation of its clients, including DDR proteins [70,71].

Synergism of cisplatin and 17AAG have been evaluated in DLBCL in our research group with data fundamental for this thesis. The data is published in the article “Hsp90 inhibition sensitizes DLBCL cells to cisplatin” [72] (Suppl. Material 1) and will briefly be presented below [72].

2. Previous results of relevance for this thesis

The experiments in this thesis are based on previously performed drug screens in a panel of DLBCL cell lines [72]. Initially, cisplatin and 17AAG single drug dose-response screens were carried out in seven DLBCL cell lines in our laboratory (Figure 5A and B) [72]. In short, the experiments were performed by seeding cells in cell line-specific concentrations, exposed to treatment for 48 hours and analyzed for cell viability using an MTS assay. Five different concentrations, each with four replicates, were used for each drug. Cell viability relative to vehicle treated control was plotted in dose-response curves (Figure 5A) and the Area Under the dose-response Curves (AUC) were estimated to rank the cell lines according to sensitivity (Figure 5B). A high AUC value indicates higher cell viability resembling cells that are more resistant to the drugs compared to the cell lines with low AUC value (Figure 5B). RIVA is one of the cell lines with the highest AUC value in contrast to SU-DHL-5 displaying one of the lowest AUC. Furthermore, RIVA and SU-DHL-5 are characterized as ABC and GCB DLBCL subclassifications, respectively, and because of the biological differences in both subclassifications and drug responses they were chosen for this thesis.

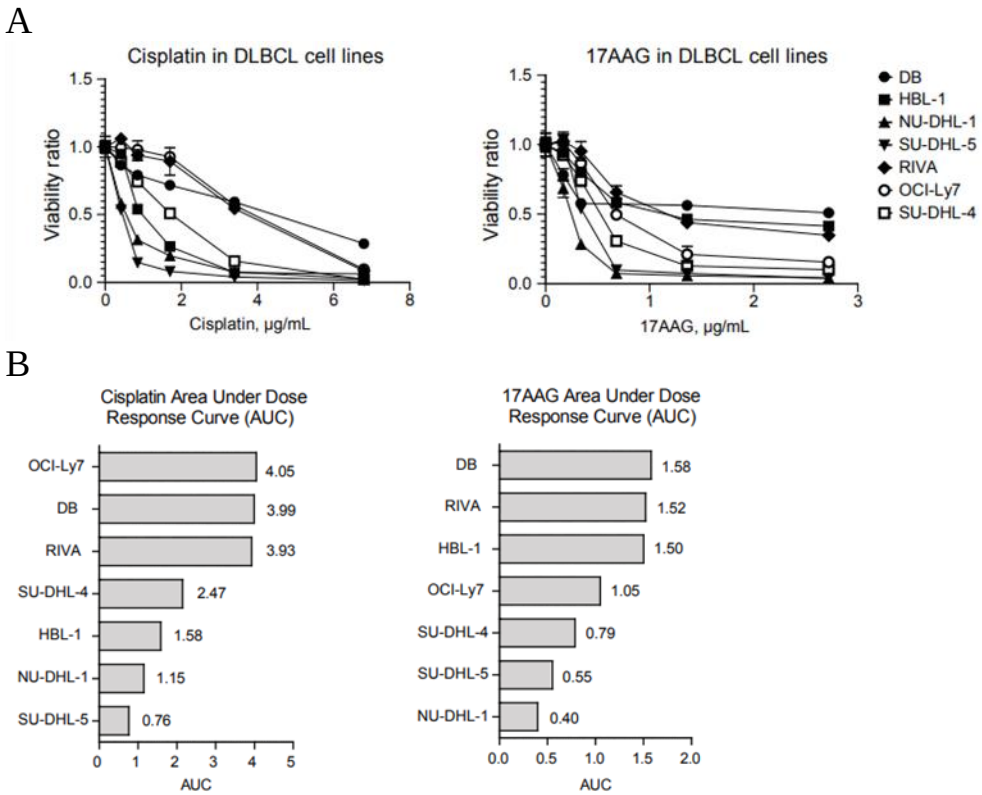

Figure 5: Cisplatin and 17AAG single drug screening in seven DLBCL cell lines. A: Dose-response curves for each DLBCL cell line for cisplatin and 17AAG, respectively. Viability ratios were estimated by response of treatment relative to vehicle controls. B: The cell lines were ranked according to AUC value after treatment of cisplatin and 17AAG, where high AUC values display better cell viability and less sensitivity to the drug, opposed to low AUC values presenting lower cell viability and more sensitivity towards cisplatin and 17AAG treatment.

As previously discussed, 17AAG indirectly effects the DDR system via inhibition of Hsp90, therefore it was tested as an add-on drug to cisplatin in the panel of seven DLBCL cell lines. To be able to analyze a broad drug interaction, cells were exposed to five drug concentrations for all cell lines, resulting in 25 (5x5) combination drug concentrations for cisplatin+17AAG for each cell line. To evaluate the synergy of the combined drugs the Bliss Independence Model was used [73,74] where the observed combination drug response (W_{AB}) was compared to the theoretical response, using the single dose responses from cisplatin and 17AAG ($W_{A+}W_B$), presented above. The drug response was estimated with cell viability assessed by an MTS assay [72]. Subsequently, Bliss score (ε) for each combination was calculated with the MTS assay values with the formula: $\varepsilon = W_{AB} - W_A W_B$. Resulting values close to zero indicates an additive effect (ε=0), a positive value resembles antagonism (ε>0) and a Bliss score with negative value indicates synergy (ε<0). The viability ratio and the calculated Bliss scores in RIVA and SU-DHL-5 are presented in Figure 6 [72]. The cisplatin and 17AAG doses giving the highest synergism for each of the cells were used in this thesis.

In summary, the presented previous results relevant for this thesis reveal the response of numerous DLBCL cell lines to cisplatin where the two cell lines used for this thesis, RIVA and SU-DHL-5 are categorized as resistant and sensitive to cisplatin, respectively. Moreover, the synergism of cisplatin and 17AAG was evaluated with MTS assay where the most synergistic doses of cisplatin and 17AAG, further used in this thesis, where identified by using Bliss Independence Model.

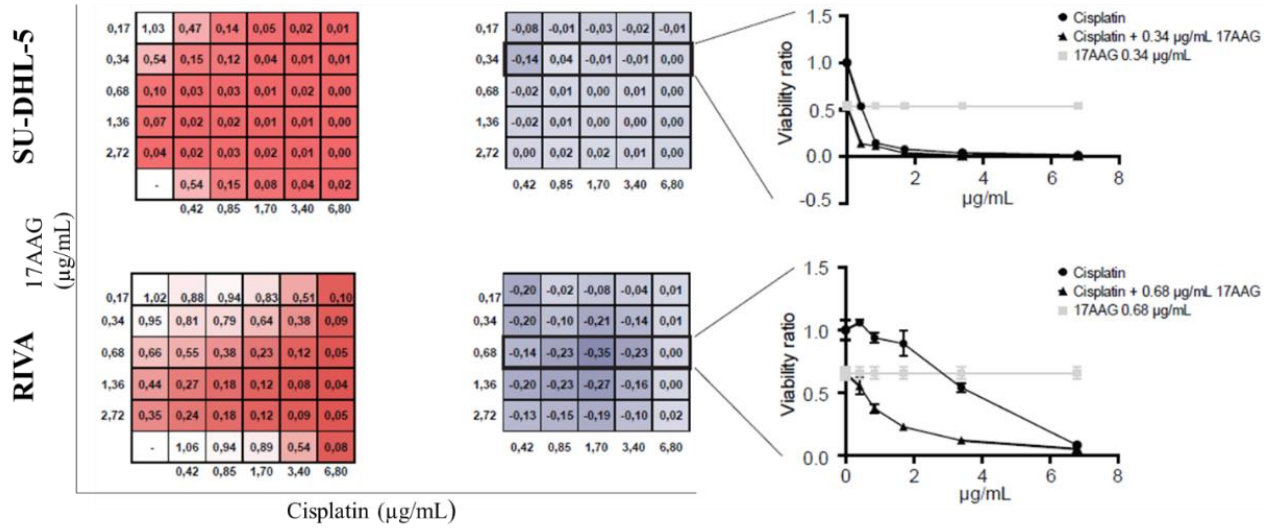

Figure 6: Drug combination viability ratios of treatment relative to control (left red panel), Bliss scores (mid blue panel) for RIVA and SU-DHL-5 along with example of dose response curves for the marked combination (right panel). The red viability panel show darker red for higher viability. The blue Bliss score panel show darker blue for low Bliss score, that is more synergy. The horizontal line (right panel) shows one 17AAG concentration and the 5 different results from this one 17AAG concentration combined with 5 cisplatin concentrations.

3. Hypothesis, aims and objectives

rrDLBCL constitute 40% of all DLBCL cases [41] and most of these patients are treated with salvage platinum-based chemotherapy [46,47] of which cisplatin is the most commonly used compound [24]. Unfortunately, a substantial subset of patients experience resistance to cisplatin and the exact molecular mechanism behind the resistance is yet to be elucidated [22,46]. However, DDR has been associated with cisplatin resistance since the DDR system is involved in cisplatin's mechanism of action [49]. 17AAG, a Hsp90 inhibitor, is suggested to affect various components of DDR and constitutes therefore a potential agent to be combined with cisplatin to overcome resistance [72].

Based on this, the main hypothesis of this thesis is that 17AAG can sensitize DLBCL cells to cisplatin, whereby cisplatin resistance can be overcome.

The overall aim is therefore to evaluate the combinatory effects of 17AAG and cisplatin treatment in DLBCL focusing on DNA damage, cell cycle progression, apoptosis, and cell viability after treatment as well as the effect on DDR protein expression after treatment.

To pursue this, experiments will be conducted in the following objectives:

- Functional assays utilizing flow cytometry to examine DNA damage, cell cycle distribution, and apoptosis, along with cell viability assay in DLBCL cell lines after treatment.
- Differential protein expression analysis of DDR related proteins in both treated and untreated DLBCL cell lines.

4. Materials & Methods

The effects of combining cisplatin and 17AAG in DLBCL were investigated with assessment of functional assays including DNA damage, cell cycle and apoptosis, analyzed with flow cytometry on two DLBCL cell lines that had been treated with both drugs. Furthermore, cell viability assay was conducted, and differential protein expression of DDR related proteins were analyzed on the treated DLBCL cell lines.

4.1 Cell lines

Two human DLBCL cell lines, RIVA and SU-DHL-5, were used for experimental analysis in this thesis. RIVA was kindly provided by Dr. Jose A. Martinez-Climent, Molecular Oncology Laboratory, University of Navarra, Spain and SU-DHL-5 was obtained from the German Collection of Microorganisms and Cell Cultures GmbH (DSMZ). RIVA and SU-DHL-5 cell lines were chosen for experimental analysis because they are different from each other regarding cisplatin response [72] and DLBCL subtype (Table 2). Both cell lines are suspension cells, cultured in growth medium consisting of RPMI-1640 complete medium (Gibco, Ref: 52400-025) supplemented with 10% (RIVA) or 20% (SU-DHL-5) Fetal Bovine Serum (FBS) (Applied Biosystems, Cat#10270106), and 1% penicillin/streptomycin (Applied Biosystems, Cat# 15140122) (Table 2). The cells were maintained at 37°C in a humidified atmosphere with 5% CO_2 and passaged every two-three days to ensure optimal cell density and access to fresh nutrients.

Cell line	Culture medium	DLBCL subtype	T2	Cisplatin response
RIVA	RPMI-1640+10% FBS+1% P/S	ABC	36 h	Resistant
SU-DHL-5	RPMI-1640+20%FBS+1% P/S	GCB	34 h	Sensitive

Table 2: Cell line characteristics. FBS: Fetal Bovine Serum. P/S: Penicillin/streptomycin. ABC: Activated B-cell like. GCB: Germinal center B-cell like. T2: Doubling time. h: hours.

At each passage the cells were counted to determine the cell viability and seeding density of the cell culture. For this a NucleoCounter NC-200 (ChemoMetec, Allerød, Denmark) was used, which is an automated cell counter. It uses Vial-Cassettes™ pre-loaded with two fluorescent dyes, Acridine Orange which stains all cells by binding to their nucleic acids and DAPI, staining dead cells with permeable cell membranes. The NucleoCounter detects the stained nuclei and analyzes a fluorescent image of the cells, recording their intensity and size [75,76]. After counting, the passage process was routinely continued by centrifuging the cell suspension at 300 g for 5 minutes to discard the old culture medium and the cell pellet was resuspended in fresh culture medium giving a cell density of 0.5×10^6 cells/mL. Each cell line culture was passaged no more than 25 times to prevent genetic

aberration that can occur with prolonged culturing [77]. Moreover, continuous culturing of the cell lines introduces the risk of cross-contamination and mycoplasma infection during routine handling, which can affect the validity of the experiments conducted using the cell lines. Accordingly, cell lines were authenticated by DNA barcoding to ensure correct cell line identity and tested for mycoplasma infection when the cell lines were thawed and brought into culture and at the end of the culturing period.

For DNA barcoding, 1 mL of the cell suspension was centrifuged at 300 g for 5 minutes, the supernatant discarded, and the pellet was washed twice with phosphate-buffered saline (PBS) (Gibco, Cat#14200-067) and stored in -20°C freezer. Upon analyzing, the pellet was thawed and used for DNA purification with DNeasy blood and tissue kit (Qiagen, Cat#69504) and subsequently used as input for amplification of the genomic DNA using AmpFISTR Identifiler polymerase chain reaction (PCR) amplification kit (Applied Biosystems, CA, USA), followed by analysis of the amplified product using capillary electrophoresis (Eurofins Medigenomix GmbH, Applied Genetics, Germany). With electrophoresis, short tandem repeats were registered and compared to the German Collection of Microorganisms and Cell Culture database [78,79] to confirm the cell line identity.

For mycoplasma screening, 1 mL of the cell suspension was centrifuged for 30 seconds at 250 g and the supernatant was kept whereas the pellet was discarded. The supernatant was centrifuged for 10 minutes at 20000 g. Hereafter, the supernatant was discarded, and the pellet was resuspended in 50 µL mycoplasma buffer (Biological Industries, Ref: 20-700-20B), heated at 95°C for 3 minutes and stored in a -20°C freezer until screening. The sample was screened for mycoplasma using PCR followed by gel electrophoresis with primers specific for the 16S rRNA gene region on mycoplasma (EZ-PCR Mycoplasma Test Kit, Biological Industries, Ref: 20-700-20).

4.2 Drug treatment of the cell lines

The effect of combining cisplatin and 17AAG was investigated by exposing RIVA and SU-DHL-5 to cisplatin alone, 17AAG alone and a combination of the two drugs. For all drug experiments, cells were seeded 24 hours prior to treatment at a concentration of 0.5×10^6 cells/mL per well in 12-well plates (Greiner Bio-One, Cat# 665180), each well containing 950 µL cell suspension with desired end volume of 1 mL, with added 50 µL of drug. Cisplatin was supplied from Aalborg Hospital in a 1 mg/mL solution in isotonic water. 17AAG was purchased from Sigma Aldrich (Cat#A8476) and supplied as 500 µg lyophilized powder. The powder was dissolved in 100 µl 100% dimethyl sulfoxide (DMSO) and aliquoted to multiple 5 mg/mL mother stocks. From this stock, an intermediate stock

with a concentration of 250 µg/mL was freshly made on the day of drug exposure to be used for experiments. Both cisplatin and 17AAG were diluted in cell culture media and then added to the wells with a cisplatin concentration of 1.7 µg/mL for RIVA and 0.415 µg/mL for SU-DHL-5 and 0.68 µg/mL 17AAG for RIVA and 0.34 µg/mL 17AAG for SU-DHL-5 (Table 3). The chosen drug concentrations were based on the most synergistic doses between cisplatin and 17AAG (Suppl. Material 1) [72]. Prior to drug experiments, the effect of DMSO (solvent for 17AAG), on cells was examined by exposing cells to the same DMSO concentration as used for 17AAG mother stocks for 48 hours, revealing no effect on the number of metabolic active cells using an MTS assay. Accordingly, vehicle controls containing DMSO and isotonic water were included for corresponding 17AAG and cisplatin treatments, respectively. The cells were subjected to drug exposure for 0, 24 and 48 hours (Table 3). At each timepoint the cells were analyzed for DNA damage, cell cycle distribution, and apoptosis with flow cytometry, as well as cell viability assay and quantitative proteomics (Figure 7).

Cell line	**Cisplatin (µg/mL)**	**17AAG (µg/mL)**	**Cisplatin+17AAG (µg/mL)**
RIVA	1.7	0.68	1.7+0.68
SU-DHL-5	0.415	0.34	0.415+0.34
Exposure time: 0, 24 and 48 hours			

Table 3: Drug concentrations and exposure times applied to RIVA and SU-DHL-5 cells.

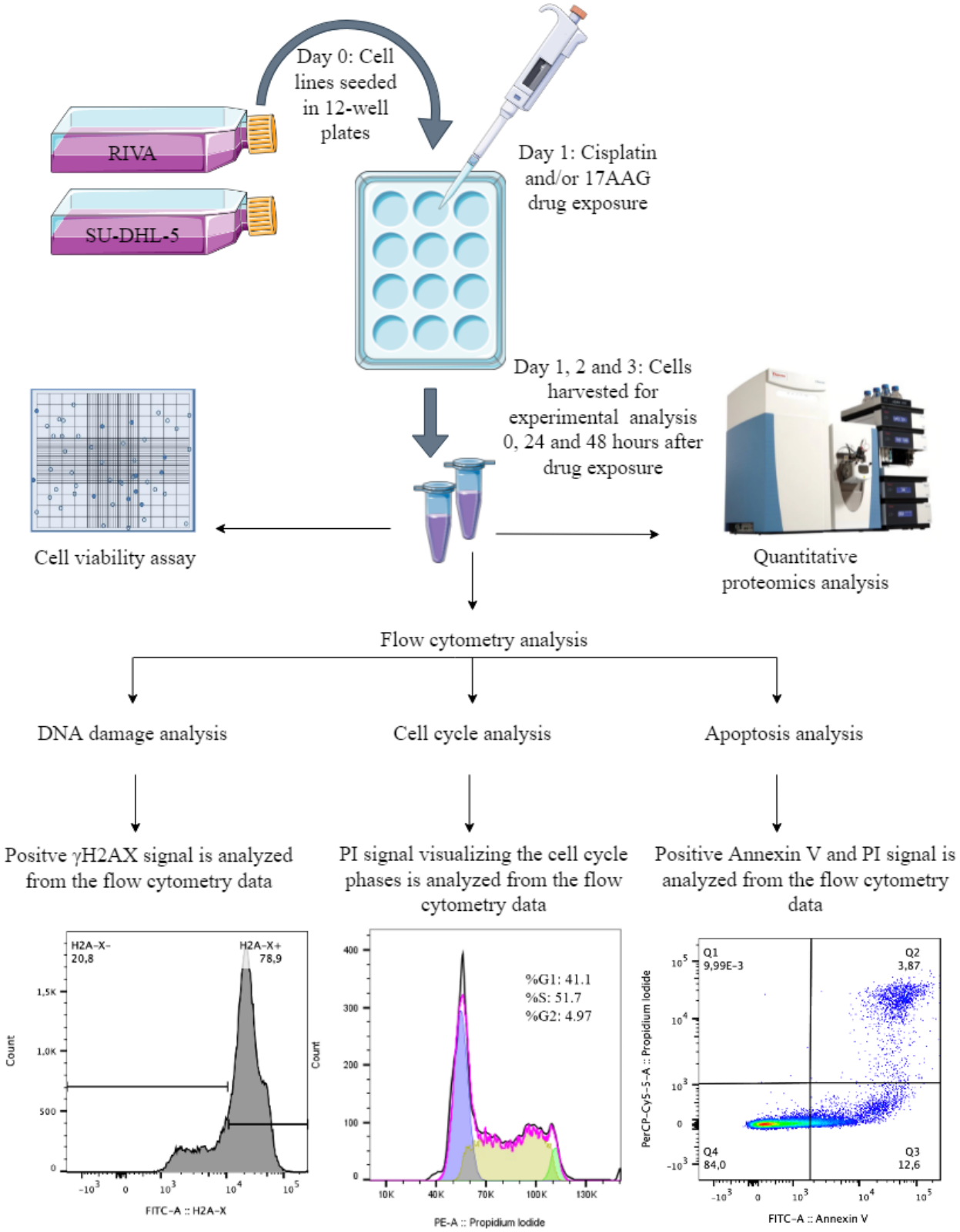

Figure 7: The workflow of the experiments conducted on RIVA and SU-DHL-5 after treatment with cisplatin and/or 17AAG. PI: Propidium Iodide. γH2AX*:* Phosphorylated histone variant H2AX.

4.3 Flow cytometry

Flow cytometry was used for DNA damage, cell cycle and apoptosis analysis of the drug treated RIVA and SU-DHL-5 cells and corresponding vehicle controls. Flow cytometry is a laser-based method that can detect and measure characteristics of particles, such as cells [80]. The procedure consists of injecting cell samples into the flow cytometer instrument where the cells flow one at a time through a laser beam, helped by a sheath fluid [81]. Light scattered from each cell is detected and measured in two different directions, forward and side, as the cells flow through the laser beam (Figure 8). These standard measurements are called the Forward Scatter (FSC), which measures the size of the cells and the Side Scatter (SSC), which measures the granularity of the cells. Additionally, each cell can be analyzed for one or multiple fluorescence parameters when the samples are stained with fluorescent dyes (e.g. Propidium Iodide) or fluorescently conjugated antibodies (e.g. Annexin FITC V) [80]. When stained cells pass through the laser in the flow cytometer, the laser light illuminates the dye molecule causing emission of light at a longer wavelength, registered by detectors. The intensity that is emitted and detected from the fluorescent dyes depends on the amount of dye or fluorochrome content in the cells and in that way can measure the amount of the targeted molecule [82]. In this study, flow cytometry was used to analyze RIVA and SU-DHL-5 cells for DNA damage with an anti-γH2AX antibody, cell cycle effect by staining with Propidium Iodide (PI) and apoptosis using an Annexin V antibody in combination with PI. All analyses were conducted on cells treated with cisplatin and/or 17AAG for 0, 24 and 48 hours. BD FACSCanto™ II Cell Analyzer (Biosciences, USA) was used for DNA damage and cell cycle analysis, whereas for the apoptosis assay a SH800S Cell Sorter, Sorting Made Simple™ (SONY) was used.

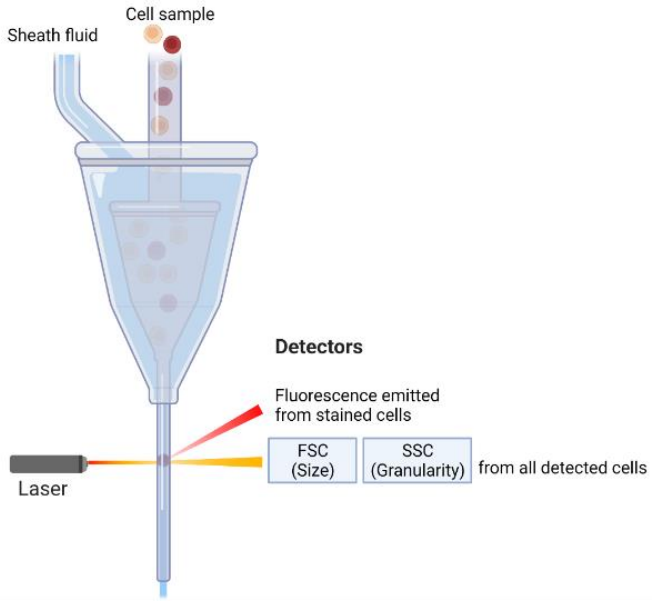

Figure 8: Simplified visualization of a flow cytometer. Sheath fluid directs the cell sample to flow past the laser beam, cell by cell. Forward Scatter (FSC) and Side Scatter (SSC) light is detected from all cells passing through the laser beam. Fluorescence emitted from stained cells are detected and quantified.

4.3.1 DNA damage analysis

After cisplatin and 17AAG exposure for 0, 24 and 48 hours, technical duplicates of the treated cell samples and one replicate of corresponding vehicle controls were fixed using ethanol. Initially, the cells were centrifuged at 400 g for 5 minutes. The supernatant was discarded, and the pellet washed once with PBS followed by second centrifugation at 350 g for 5 minutes. The supernatant was discarded, and 70% ethanol was added to the pellet drop by drop while vortexing. The fixed cells were then incubated at -20°C for at least 60 minutes before staining.

For detection of DNA damage, a FITC anti-H2A.X Phospho (ser139) antibody (anti-γH2AX antibody) (Biolegend, Cat#613404) was used. When dsDNA damage occur in mammalian cells, the H2AX subtype of histone H2A becomes phosphorylated in the Ser139 residue [83,84]. Thus, the phosphorylated H2AX, also called γH2AX, can be used as a marker for quantifying DNA damage in the form of DSBs in cells and tissues [84]. To stain the cell samples with γH2AX antibody, the fixed cells were washed three times with staining buffer (BD Pharmingen, Cat#554657) and centrifuged at 350 g for 10 minutes after each wash. Samples were then resuspended in 100 µL consisting of 2.5 µL anti-γH2AX antibody and 97.5 µL staining buffer and subsequently incubated for 45 minutes at 4°C in the dark. After incubation, the samples were washed twice with staining buffer to remove unbound antibody and then resuspended in 300 µL staining buffer for flow cytometry.

The γH2AX antibody concentration was determined by performing antibody titrations with dilution series of 1:1, 1:2, 1:4, 1:8, 1:16 and 1:32, followed by calculating which dilution had the highest staining index (Suppl. Figure 1 and Suppl. Table 1).

4.3.2 Cell cycle analysis

When samples had been analyzed for DNA damage with γH2AX antibody staining, the remaining ethanol fixed cells in the samples were used for analysis of cell cycle distribution. The technical duplicates of each sample were centrifuged at 350 g for 10 minutes and resuspended in 250 µL staining buffer, followed by addition of 1 µL 100 mg/mL Ribonuclease A solution (QIAGEN, cat#69504) to each sample and incubation for 30 minutes at 37°C to degrade RNA in the samples. Subsequently, 5 µL PI (Biolegend, Cat#421301) was added to each sample and samples were analyzed on the flow cytometer. PI is a fluorescent intercalating agent that binds to both DNA and RNA, hence the RNase treatment. Once PI is bound to DNA by intercalating between base pairs it emits light at 488-617 nm after excitation, whereby the DNA content of each cell can be quantified. At each cell cycle a somatic diploid (2n) cell will prepare for DNA synthesis in G1-phase and proceed

to DNA replication in the S-phase where the cell doubles its amount of DNA (to 4n) prior to the G2- and M-phase. Therefore, the quantified DNA content by PI can define the cell cycle phases of the cell population [83–86].

4.3.3 Apoptosis analysis

The apoptosis analysis was performed by staining the cell samples with FITC Annexin V (Biolegend, Cat#640906) and PI. Annexin V is a cellular protein which binds to phosphatidylserine on the surface of apoptotic cells in a calcium-dependent manner. Normally, phosphatidylserine is found intracellularly but during early apoptosis the membrane becomes more asymmetric resulting in phosphatidylserine translocation to the external surface of the cell. In that way, Annexin V is an excellent marker for identifying and measuring early apoptotic cells [85]. PI is often used in combination with Annexin V for apoptosis analysis. PI binds to nucleic acids of dead or fixed cells with permeable cell membranes, but do not enter viable or early apoptotic cells with intact plasma membranes. Therefore, PI can be used as a viability marker and in conjunction with Annexin V, PI makes it possible to distinct early apoptotic cells (Annexin V+, PI-) from late apoptotic (Annexin V+, PI+) and necrotic cells (Annexin V-, PI+) [86].

Technical duplicates of samples treated with cisplatin and/or 17AAG and vehicle controls, along with four heat-induced positive control samples were used for the analysis. The heat-induced samples had been incubated at 60°C for 15 minutes to induce apoptosis and were used as positive controls. One of the four samples was left unstained while the other three samples were stained with only Annexin V, only PI, and both Annexin V and PI, respectively (Suppl. Figure 2). The cisplatin and/or 17AAG treated samples and the vehicle controls were stained with both Annexin V and PI. Briefly, all the samples were freshly harvested and centrifuged for 5 minutes at 300 g, followed by a washing step with PBS. After a second centrifugation the supernatant was discarded, and the cells were resuspended in a FACS tube with Annexin V Binding Buffer (Biolegend, Cat#422201). To the FACS tubes, 5 µL FITC Annexin V and PI were added, resulting in a staining volume of 110 µL. After staining, the samples were incubated for 20 minutes at room temperature in the dark. Hereafter, 400 µL Annexin Binding Buffer was added and the cells were analyzed immediately on the flow cytometer.

4.3.4 Analysis of flow cytometry using FlowJo

The program FlowJo v.10.7.1 was used to analyze the flow cytometry output. For each experiment, data analysis with a specific gating strategy was used to get a filtered output. First, the cell population of interest was identified. For the DNA damage and cell cycle analysis the viable cell population was of interest and apoptotic cells were filtered out along with debris. On the contrary, the apoptotic cells were of interest for the apoptosis analysis where only debris was filtered out. The gated cell population in each experiment was then plotted to discriminate doublets from singlets where gating was performed to exclusively include single cells. This filtered population was used to analyze the intensity of the stained samples (Figure 9).

For the DNA damage analysis, the negative controls (without antibody), presenting the true negative γH2AX intensity signals were used to determine the cutoff between negative and positive γH2AX intensity signals from the treated samples and vehicle controls. In that way, all γH2AX signals above the negative control signal were regarded as positive γH2AX signal in the samples.

The fluorescence signal emitted from PI in the cell cycle analysis was analyzed by plotting the PI intensity which peaks of intensity indicates G1 and G2/M phases of the cell cycle. The signals between the two peaks indicate the S phase of the cell cycle. An univariate cell cycle model with Watson Pragmatic algorithm was used to automatically gate the cell cycle phases for SU-DHL-5. In contrast, the RIVA cells were manually gated due to the extreme effect of cisplatin on the cell cycle that hindered the algorithm to recognize the cell cycle phases.

For the apoptosis analysis, Annexin V and PI fluorescence intensities were analyzed by an Annexin V vs. PI plot. The margins for Q1, Q2, Q3 and Q4, were determined from the analysis of the heat-induced apoptotic positive controls (Suppl. Figure 2). Q1 presents PI positive (necrotic cells), Q2 presents Annexin C and PI positive (late apoptotic cells), Q3 presents Annexin positive cells (early apoptotic cells) and Q4 presents viable cells, negative for both.

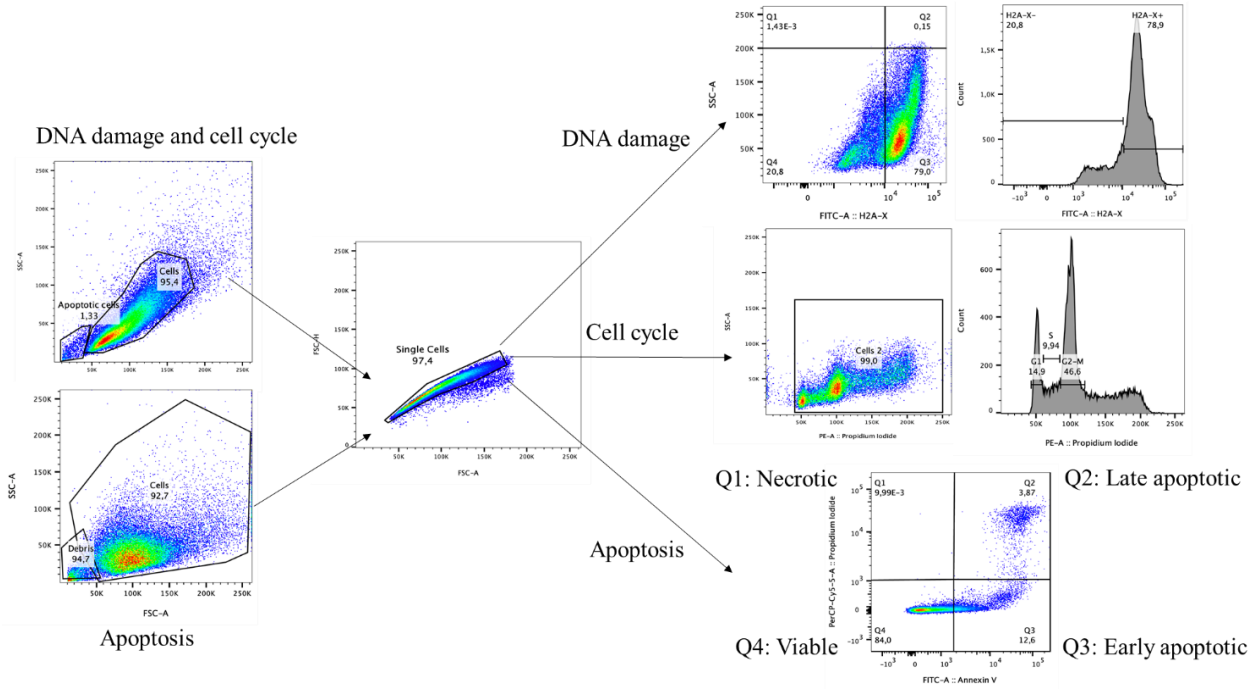

Figure 9: Overview of the gating strategy conducted on the flow cytometry analyzed cell samples resulting in filtered population that was analyzed for staining intensity.

4.4 Cell viability assay

Cell counting analysis was performed to elucidate the viability of the cell lines at each timepoints after the different treatment exposures, in duplicates. Trypan blue exclusion assay was performed to identify and count both live and dead cells. A cell suspension aliquot was diluted 1:1 with Trypan Blue Solution (Gibco, Cat# 15250061) and pipetted on a hemocytometer and placed under Nikon Eclipse TS100 light microscope. In this assay the dye is only taken up by dead cells as their membrane is disrupted and permeable, differentiating them from live cells. The hemocytometer is constructed with four chambers with grids to ease the manual counting. If total live cell count were >100 in the first two chambers of the hemocytometer, an average of the cell count from these two chambers were used, whereas average of cell count from all four chambers were used if the total live cell count of the first two chambers were <100. Nucleocounter NC-200 was also used to count total cells and live cells to validate and compare with cell count from the hemocytometer.

4.5 Proteomics

4.5.1 Sample preparation for protein analysis

RIVA and SU-DHL-5 cell samples were harvested after 0, 24 and 48 hours of cisplatin and/or 17AAG exposure along with vehicle controls for differential protein analysis. The harvesting of the samples included washing with centrifugation steps at 300 g for 5 minutes, followed by pipetting 10 µL 1 M

triethylammonium bicarbonate (TEAB) (Sigma Aldrich, CAS#15715-58-9) to the cell pellets that were subsequently stored in -80°C freezer until use for mass spectrometry. To be able to analyze on the mass spectrometer, the samples were prepared by digesting the proteins into smaller peptides. First 50 µL 0.1% RapiGest were added to the frozen samples and then heated to 60°C for 10 minutes, followed by sonicating for 15 minutes to denature proteins. This was followed by centrifugation at 15000 g for 5 minutes to sediment any insoluble material resulting in a visible pellet. The supernatant was transferred to a LoBind Tube. Hereafter, 1.2 µL of Tris (2-carboxyethyl) phosphine hydrochlorid (Sigma-Aldrich, CAS#51805-45-9) and 6 µL of 0.5 M chloroacetamide was added pr. 50 µL sample, followed by incubation for 30 minutes at 37°C. After incubation, 0.5 µg trypsin in 50 mM TEAB was added, now incubated at 37°C overnight. The day after, 1 µL of 100% Trifluoroacetic acid (Thermo Fisher, CAT#85183) was added, and the samples were incubated at 37°C for 30 minutes. Now the samples consisted of small peptides which concentrations were detected before it was used for liquid chromatography tandem mass spectrometry (LC-MS/MS).

4.5.2 LC-MS/MS data acquisition

Two replicates of each sample, each containing 500 ng of peptides was injected onto Dionex Ultimate 3000 nanoLC (Dionex and Thermo Scientific, Waltham, USA) system, connected to timsTOF Pro (Bruker, USA) mass spectrometer equipped with CaptiveSpray ion source (Bruker, USA). The samples were loaded with 60-minute gradient to a 25 cm IonOpticks column. Two LC buffers were used, buffer A (0.1% formic acid (FA)) and buffer B (99.9% Acetonitrile (AcN) 0.1% FA). The resulting quantitative proteome analysis provides the mass-to-charge ratios of the precursor peptides (MS1) and the fragments generated from these peptides (MS2). The two mass spectra could then be investigated, and proteins identified using search engines that matched the two MS spectra to protein sequence databases, described below.

4.5.3 Protein identification and Quantification

Spectronaut (v. 15) was used for protein identification. The program searches the data from the mass spectra against Uniprot human protein sequence database (10. January 2022; human reference proteome). Settings in Spectronaut included the Protein Quant 2.0 algorithm, peptide and protein FDR of 1% and at least two peptides matched for protein quantification. Reversed sequences as decoys were filtered automatically by Spectronaut.

4.5.4 Protein data processing and data analysis

The output data from Spectronaut was processed and analyzed in the computer software Perseus (v.1.6.10.43). Proteins identified were in total 5429 for all RIVA and SU-DHL-5 samples before filtering. The samples were categorized into replicates and cell lines, followed by calculating the quantitative protein value average of both replicates for each sample. Each protein from the MaxQuant/Spectronaut LFQ were log2 transformed whereafter histograms were made presenting the intensities of each sample for visualization and ensuring normally distributed data. Hereafter, missing values were imputed from a normal distribution and potentially contaminated hits were filtered by manually selecting all keratin variants that are thought to come from skin, hair, or nails under sample preparation. Ultimately, the quantitative protein values for DDR proteins of interest were extracted from Perseus to be analyzed for expression differences after drug treatment.

4.6 Statistical analysis

Statistical analysis and graphs, presenting data from flow cytometry analyses, cell viability assay and proteomics were performed and constructed with GraphPad Prism v.8. The DNA damage analysis was performed with four biological replicates, whereas the cell cycle analysis and apoptosis assay were performed in biological duplicates. The cell viability assay and quantitative proteomic analysis was performed in one biological duplicate (Suppl. Table 2-6). One representative biological replicate for each experiment will be presented in the results were each include technical duplicates of all samples, except for the vehicle samples in the DNA damage analysis. Statistical analysis was performed with two-way Analysis of variance (ANOVA) with multiple comparisons where treatment parameters of cisplatin single drug, 17AAG single drug, combination of cisplatin and 17AAG and vehicle controls were all compared for effect on DNA damage, cell cycle distribution, apoptosis, cell viability and expression of DDR proteins. The significant differences are presented on the graphs with * symbols, where *$p \leq 0.05$, ** $p \leq 0.01$, *** $p \leq 0.001$, and **** $p \leq 0.0001$.

5. Results

The main mechanism of action of cisplatin is induction of DNA adducts and double stranded DNA (dsDNA) breaks that can trigger cell cycle arrest, ultimately leading to apoptosis [50]. Resistance to this effective antitumor agent has been associated with dysfunctional DDR that can repair the cisplatin-induced DNA damage and prevent apoptosis of the cancer cells. Therefore, inhibition of DDR during cisplatin exposure have been proposed to enhance its cytotoxic effects. 17AAG, a suggested indirect DDR inhibitor, have been found to act synergistically with cisplatin. To evaluate the molecular effects behind the synergism, this thesis investigated DNA damage, cell cycle distribution, apoptosis activity, cell viability and quantitative proteome analysis of DDR related proteins, upon treatment with cisplatin and 17AAG as single drugs and in combination, along with corresponding vehicle controls. The occurrence and distribution over time of these effects were investigated in two different DLBCL cell lines, RIVA and SU-DHL-5, which have been categorized as resistant and sensitive to cisplatin, respectively (Suppl. Material 1) [72]. Optimization experiments were initially conducted and evaluated for acquisition of the most optimal experimental setup of the final experiments presented in this chapter where each final experiment represent one biological replicate. All experiments are listed in Suppl. Table 2-6.

5.1 Combinatory treatment enhances cisplatin induced dsDNA damage in RIVA

Drug induced DNA damage in terms of dsDNA breaks were investigated in cisplatin- and/or 17AAG-exposed RIVA and SU-DHL-5 cells, along with vehicle controls, by γH2AX signal quantification with flow cytometry. One plausible confounding factor in the experimental set up was that apoptosis can induce DNA fragmentation that results in dsDNA breaks thus also emitting γH2AX signal [87,88]. To take this in to account, an initial experimental setup was performed where γH2AX was quantified 4 and 8 hours after cisplatin exposure which is limited time for cells to have undergone apoptosis. In this experiment, both RIVA and SU-DHL-5 cells showed increased percentage of γH2AX positive cells compared to the vehicle control already after 4 and 8 hours implying that the γH2AX signal was caused by cisplatin-induced DNA damage and not apoptosis-induced DNA fragmentation (Suppl. Figure 3-4). Additionally, cisplatin induced DNA damage in a time dependent manner with 24.4%, 56.4%, and 78.9% γH2AX positive RIVA cells after 4, 8 and 24 hours, respectively (Suppl. Figure 3). The same tendency was observed for SU-DHL-5 (Suppl. Figure 4) and therefore longer time exposure were chosen in the following experiments i.e., 24 and 48 hours, along with 0 hours for baseline reference. The most synergistic doses for each cell line were chosen based on previous MTS assay and Bliss score results [72] and used for final subsequent experiments

with cisplatin concentrations of 1.7 µg/mL for RIVA and 0.415 µg/mL for SU-DHL-5 as well as 0.68 µg/mL 17AAG for RIVA and 0.34 µg/mL 17AAG for SU-DHL-5, along with vehicle controls. The dsDNA damage experiment was conducted in biological quadruplicate (Suppl. Table 2) each containing technical duplicates except for the vehicle control which only contains one technical replicate. The following results were based on the technical duplicates of the final experiment (one representative biological replicate).

The defined cut-off based on unstained samples divided the fluorescence signal of each sample into positive (γH2AX+) and negative (γH2AX-) populations (Figure 10A and D, Suppl. Figure 5-6). Percentages of counts included in the γH2AX+ populations were plotted in histograms (Figure 10B and E) enabling direct comparison between treatments at individual time point. All 0-hour samples presented very similar γH2AX+ percentages documenting valid baseline values prior to the drug effects (Figure 10B and E).

In RIVA cells, high percentages of dsDNA damage were generally observed in cisplatin and combination treated cells at both 24 and 48 hours with a total range of 51.9-88.8% γH2AX+ cells (Figure 10B, Suppl. Figure 5). These could not be statistically compared with the vehicle control as the control only contained one replicate. However, both cisplatin- and combination-treated RIVA cells showed statistically higher γH2AX+ compared to 17AAG after 24 and 48 hours (Figure 10B), implying that the DNA damage detected through γH2AX was induced primarily by cisplatin. In RIVA cells, no significant differences of the percentages of γH2AX+ cells after cisplatin treatment compared to combination treatment was observed (Figure 10B). On the contrary, the left γH2AX fluorescence intensity histogram (Figure 10A) showed that the combination treatment have higher γH2AX intensity compared to cisplatin alone which indicates higher number of γH2AX foci per cell and thus a higher total degree of DNA damage [72]. To visualize this, mean intensities of γH2AX+ populations were plotted for both cell lines (Figure 10C and F) and showed significantly higher γH2AX+ level after 24 and 48 hours of combination treatment, compared to cisplatin single drug treatment (approximately 1,5-fold change at both timepoints). This supports that cisplatin induced DNA damage in cisplatin-resistant RIVA cells is increased when combined with 17AAG.

In SU-DHL-5 cells, single drug treatment of cisplatin had the highest amount of γH2AX+ percentages after both 24 hours (44.2-45.7%) and 48 hours (31.4-36.3%) of treatment exposure with significantly higher percentage compared to combination after 24 and 48 hours (Figure 10E and Suppl. Figure 6). Thus, these results suggest that the DNA damage effect of cisplatin on SU-DHL-5 is highest when

given as single drug and that the combination of cisplatin and 17AAG does not have a synergistic DNA damage effect in SU-DHL-5 cells, contrary to RIVA which moreover suggests a cell type specific effect of 17AAG as the addition of 17AAG did not enhance cisplatin-induced DNA damage at used concentrations in SU-DHL-5. In accordance with RIVA cells, 17AAG single drug did not show noticeable effect on DNA damage with significant lower γH2AX+ percentages, compared to combination after 24 hours and compared to cisplatin after 48 hours (Figure 10E). This emphasizes that 17AAG alone is not responsible for induction of DNA damage. Oppose to RIVA cells, SU-DHL-5 cells showed no significant differences of the mean intensities of γH2AX+ population (Figure 10F).

In summary, cisplatin-induced DNA damage in form of dsDNA breaks were detected through anti-γH2AX staining with high amount of γH2AX+ population after treatment with cisplatin as single drug in both cell lines. The DNA damage was observed as soon as 4 hours after drug exposure, thus supporting that cisplatin induces dsDNA breaks prior to induced apoptosis. The combination of cisplatin and 17AAG showed increased DNA damaging effect in RIVA cells, compared to cisplatin single drug visualized by the difference of the mean intensity of γH2AX+ between cisplatin and combination. This suggests that the synergism of cisplatin and 17AAG can at least partially be based on the enhancement of DNA damage, which is however, not observed in SU-DHL-5, thus, exhibiting cell type specific synergistic effects.

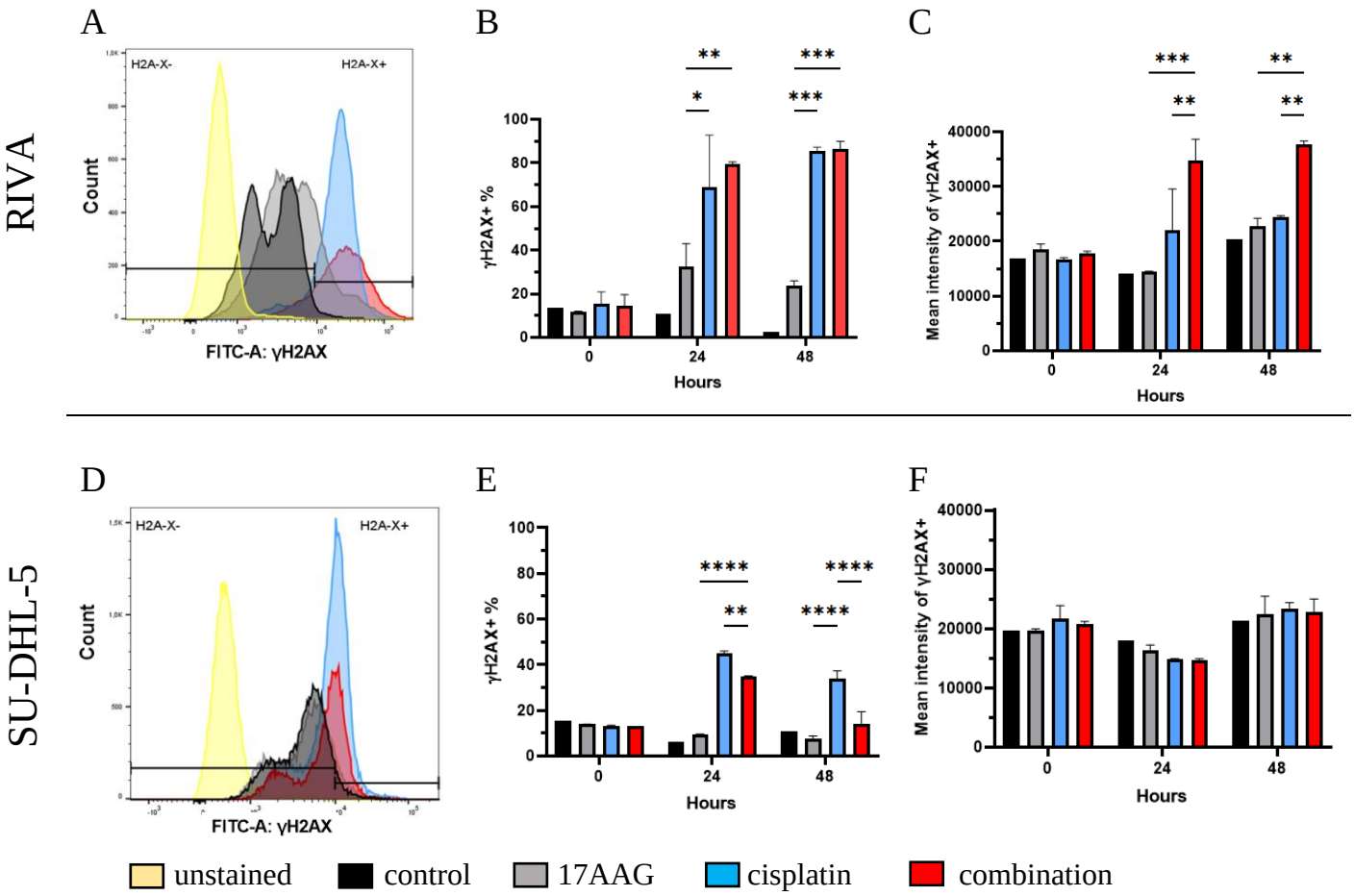

Figure 10: DNA damage measured by anti-γH2AX staining in RIVA and SU-DHL-5 treated with cisplatin and 17AAG as single drugs and in combination for 0, 24 and 48 hours, along with vehicle controls. **A and D:** Representative samples of fluorescent γH2AX intensity histograms showing an unstained sample as well as all 24- and 48-hour treated and vehicle SU-DHL-5 and RIVA samples, respectively. The plotted cut-off based on the unstained sample, defines positive (γH2AX+) and negative (γH2AX-) populations. The fluorescent γH2AX intensity histograms of the other samples are presented in Suppl. Figure 5 and 6. **B and E:** Percentages of γH2AX+ cells in each drug and vehicle treated samples at each timepoint. **C and F:** Mean intensity of γH2AX+ signals emitted in all samples.
Two-way ANOVA was used to compare all treatments at each timepoint. The experiment was conducted in biological quadruplicate and technical duplicate except for the vehicle control sample containing only one replicate and was therefore not qualified for statistical analysis. Significant differences are showed with: *p value≤ 0.05, ** p value≤ 0.01, *** p value≤ 0.001, and **** p value≤ 0.0001.

5.2 Cisplatin disrupted the cell cycle distribution of RIVA and SU-DHL-5

Cell cycle distribution was investigated in RIVA and SU-DHL-5 after treatment with cisplatin and 17AAG as single drugs and combination of the two drugs, along with vehicle controls, using PI staining and subsequent flow cytometry. Cell cycle algorithm models, automatically defining the distribution of cells in the G1-, S-, and G2/M-phases of the cell cycle based on PI staining are commercially available. However, RIVA cells treated with cisplatin at used concentrations for 24 and

48 hours revealed highly affected cell cycle distribution due to the high levels of DNA damage (Suppl. Figure 7), which hindered the algorithm to recognize the cell cycle phases. Therefore, the subsequently presented results of cisplatin's effect on cell cycle distribution in RIVA will only be analyzed in a qualitative manner. In contrast, less DNA damage was induced in SU-DHL-5 with less affected cell cycle distribution (Suppl. Figure 8) and therefore a univariate cell cycle model with Watson Pragmatic algorithm available in FlowJo was applied for defining the cell cycle phases in SU-DHL-5 cells. This analysis was conducted in biological duplicates (Suppl. Table 3) each containing technical duplicates where following results contain the technical duplicates of one representative biological replicate.

The PI intensity histograms in Figure 11A show the effect on cell cycle of drug and vehicle treated RIVA cells after 48 hours with noticeable disturbed cell cycle distribution in cisplatin single drug treated cells. The first peak on the graph indicates G1-phase, however it is difficult to define and distinguish the S- and G2/M-phases. Additionally, the histograms present a post-G2/M phase in the vehicle control (Figure 11A) which plausibly show the biological aneuploidi of RIVA cells. Same tendencies of cell cycle phase distributions were noticed for both cisplatin- and combination-treated RIVA cells at 24 hours (Suppl. Figure 7B). The indistinguishable S- and G2/M-phases support the DNA damage results presented above exhibiting high levels of cisplatin-induced DNA damage at both timepoint as this intercalating effect of cisplatin is suggested to mainly affect the S and G2/M cell cycle phases [89]. The intercalating effect resulting in DNA damage can activate cell cycle checkpoints that delay cell cycle progression to gain time for DDR, making cells stuck in these phases leading to increased number of cells in the S- and G2/M-phases [49]. This is further suggested with the presented bar plots where the most prominent difference was the increase of G2-phase in cisplatin and cisplatin combined with 17AAG treated RIVA samples for 48 hours (Figure 11B). Furthermore, the bar plots show a general effect on the cell cycle after 24 and 48 hours where the drug treated RIVA cells display differences of cell cycle phase distribution compared to the corresponding vehicle samples which is not present in the baseline 0-hour exposure (Figure 11B).

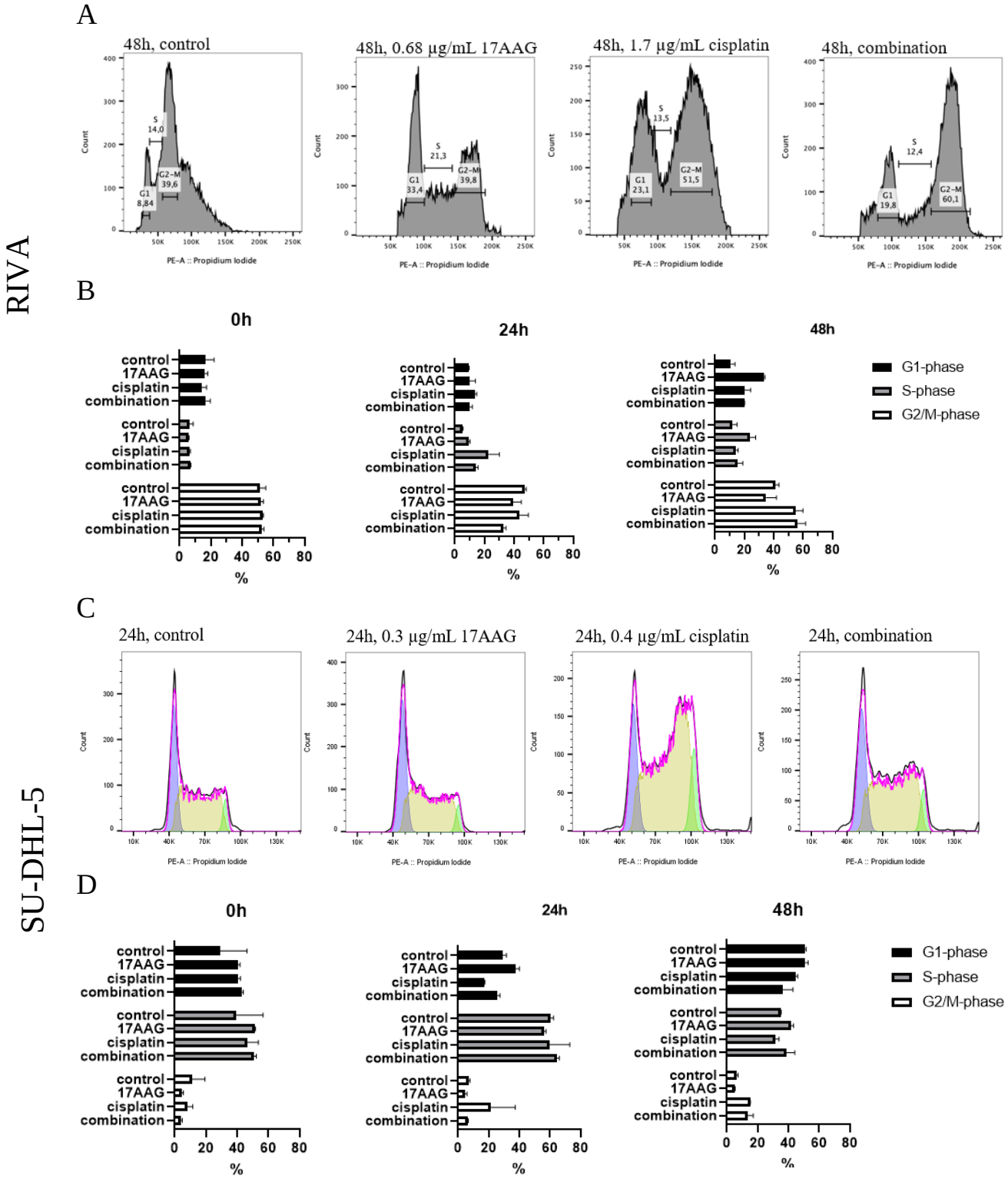

Figure 11: Effect of cisplatin and 17AAG on RIVA and SU-DHL-5 cell cycle distribution after treatment as single drugs and in combination, along with vehicle controls. **A and C**: Propidium Iodide intensity histograms presenting DNA content of the cells and thereby cell cycle phases that were manually guided for RIVA and automatically guided with univariate cell cycle model using Watson Pragmatic algorithm for SU-DHL-5. **B and D:** Bar plots presenting the cell cycle distribution in percentages for the duplicate average of each sample. Statistical analysis were not conducted between the cell cycle distribution after treatment/vehicle due to the uncertainty of the actual values.

In SU-DHL-5, the univariate cell cycle model showed disruption of the cell cycle distribution after cisplatin treatment for 24 hours, as observed in RIVA cells (Figure 11C). Furthermore, the analysis showed increased percentages of cells in G2-phase after cisplatin single drug exposure for 24 hours as well as for cisplatin and combination treatment for 48 hours, compared to corresponding controls (Figure 11D) which is comparable to the cell cycle distribution of cisplatin treated RIVA cells. Generally, the highest effect on the cell cycle distribution was seen in SU-DHL-5 after cisplatin single drug treatment for 24 hours with increased G2-phase constituting up to 32.2% of the cells, compared to corresponding vehicle control constituting up to 7.93% of the cells in G2-phase (Figure 11D and Suppl. Figure 8B). This shows that 17AAG does not enhance the effect of cisplatin on cell cycle distribution which is in accordance with the previous DNA damage results in SU-DHL-5.

Even though the cell cycle phases are difficult to distinguish from each other, especially for RIVA, the results support that cisplatin alters the cell cycle distribution of RIVA and SU-DHL-5 through induction of DNA damage with cell cycle arrest in post G1-phase.

5.3 Cisplatin and 17AAG showed synergistic effects on apoptosis in RIVA cells

To investigate RIVA and SU-DHL-5 cells for apoptotic response to cisplatin as a single drug and in combination with 17AAG, the treatment exposed cells were, along with vehicle controls, stained with Annexin V and PI and analyzed with flow cytometry. The cell population in each replicate were distributed into necrotic (Q1), late apoptotic (Q2), early apoptotic (Q3), and viable cells (Q4) that were defined by gating positive controls for Annexin V and PI (Suppl. Figure 2 and 9-10). In that way, the percentages of cells present in each quadrant were found as presented in Figure 12A-B with representative 24- and 48-hour samples for SU-DHL-5 and RIVA, respectively.

Noticeably, SU-DHL-5 cells had large amount of early apoptotic cells in vehicle controls after 24 and 48 hours (Figure 12B and Suppl. Figure 10) and in all samples after 0 hours of drug exposure (Suppl. Figure 10) stating high apoptotic levels in unaffected SU-DHL-5 cells not exhibited in RIVA. Both biological duplicates of this experiment resulted in analog results with high levels of apoptotic cells in unaffected SU-DHL-5 cells and not in unaffected RIVA cells which suggests a biological baseline pro-apoptotic disturbance in SU-DHL-5 cell line. For all treated samples at the different time points, <2% of the cells were detected in late apoptotic (Q2) and necrotic phases (Q1), while the largest effect of drug treatment was observed in the percentage of early apoptotic cells (Q3) (Suppl. Figure 9-10). The replicative average percentages of each quadrant were used to calculate the levels of apoptotic

cells (both early: Q3 and late: Q2) in drug affected samples relative to vehicle controls at each timepoint (Figure 12C-D)

For RIVA cells, exposure of all drug treatments for 24 and 48 hours showed significantly higher level of apoptotic cells compared to corresponding vehicle treatment, with most prominent difference in combination treatment for 48 hours constituting approximately seven-fold increase, compared to corresponding vehicle control (Figure 12C). Furthermore, the combination treatment showed significantly higher levels of apoptotic cells compared to cisplatin single drug treatment alone after both 24 and 48 hours of drug exposure, suggesting a synergistic effect of cisplatin and 17AAG on apoptosis in RIVA cells (Figure 12C) which is in accordance with their synergistic effect on induction of dsDNA damage presented above.

In SU-DHL-5 the apoptotic levels were not as affected by drug exposure as seen for RIVA. However, statistically higher levels of apoptotic cells were seen for all 24-hour drug treated cells, compared to corresponding vehicle control, where the combination constituted the highest level with approximately two-fold change (Figure 12D). The lower apoptotic effect of cisplatin and 17AAG on SU-DHL-5, compared to RIVA, could be explained in the high number of apoptotic cells in unaffected cells, masking the apoptotic effect of cisplatin.

As for the dsDNA damage results in RIVA, the apoptotic assay displayed results that support the supposition of the synergistic effects of cisplatin and 17AAG, having increased cytotoxic effect compared to cisplatin alone in RIVA and with less confidence in SU-DHL-5. The aberrant levels of apoptotic cells in unaffected SU-DHL-5 cells raised the question if the early apoptotic cells do present cells that will in fact terminate the apoptotic process and die. Therefore, a cell viability assay was conducted for SU-DHL-5 and RIVA vehicle samples and cisplatin and/or 17AAG treated samples.

A – RIVA

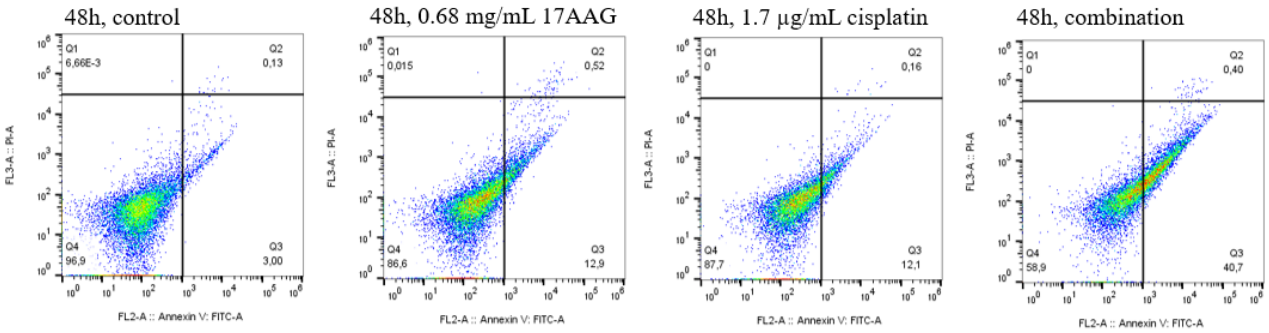

B – SU-DHL-5

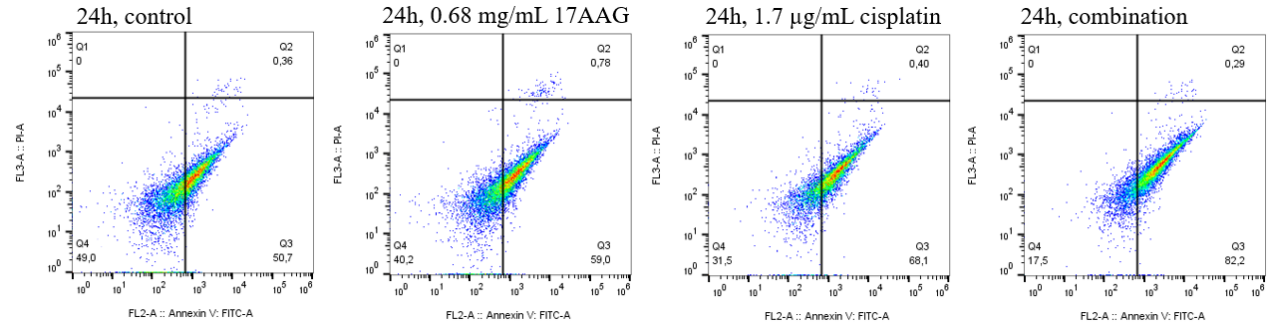

C

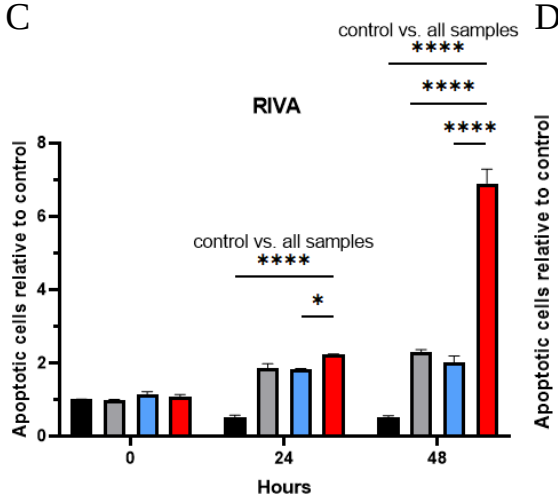

D

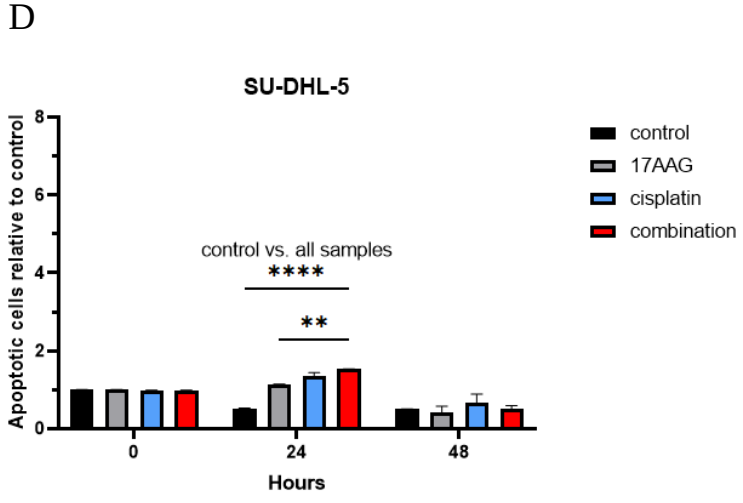

Figure 12: Effect on apoptosis in RIVA and SU-DHL-5 after cisplatin and/or 17AAG treatment. **A and B:** Intensity plot of Annexin V (x-axis) and PI (y-axis) with gated defined apoptotic phases; necrotic (Q1), late apoptotic (Q2), early apoptotic (Q3) and viable cells (Q4). **C and D:** Histograms of the early and late apoptotic cells (Annexin positively stained) in each drug treated sample (average of duplicate) relative to vehicle sample (average of duplicate) at each time point. Two-way ANOVA with multiple comparisons was used for statistical analysis, *p value≤0.05, **p value≤0.01, ****p value≤0.0001.

5.4 Cell viability of RIVA and SU-DHL-5 was affected by cisplatin treatment

To investigate the cell viability of SU-DHL-5 and RIVA cell lines after single drug and combination treatment of cisplatin and 17AAG for 0, 24 and 48 hours, along with vehicle controls, the cells in each duplicate in each sample were counted with both hemocytometer and nucleocounter NC-200, at each timepoint (Figure 13 and Suppl. Table 7-8). All samples harvested after 0 hours of treatment showed similar cell viability (Figure 13A-B). When both RIVA and SU-DHL-5 cells had been treated with cisplatin as single drug and in combination with 17AAG for 24 and 48 hours, the cell viability was significantly lower compared to vehicle controls (Figure 13A-B), with most apparent difference in SU-DHL-5 after 48 hours of drug (Figure 13B). This is interesting since the cellular effects of cisplatin on SU-DHL-5 in the results above are not as prominent as in RIVA. Moreover, the SU-DHL-5 vehicle treated samples previously shown to have large amount of early apoptotic cells distinctly increased the cell viability with time, opposed to cisplatin and combination treated samples (Figure 13B). This indicates that the early apoptotic SU-DHL-5 cells in vehicle treated samples presented in the results for the apoptotic assay do not present the number of cells that will terminate the apoptosis process rather it present cells that have a biologically pro-apoptotic SU-DHL-5 cell-specific characteristics that do not affect the survival of the cells.

In summary, cisplatin exposure affected DNA damage, cell cycle distribution, apoptosis and cell viability in both RIVA and SU-DHL-5 and by combining cisplatin with 17AAG, these effects were enhanced in RIVA, especially for apoptosis, suggesting cell line specific synergism of cisplatin and 17AAG. However, the presented results above showed only a general phenotypic cellular response towards the combination and to gain deeper molecular understanding of the suggested synergism of cisplatin and 17AAG, the DDR mechanism involved in mechanism of action of both drugs, was investigated by analyzing proteomics of DDR proteins.

RIVA
A

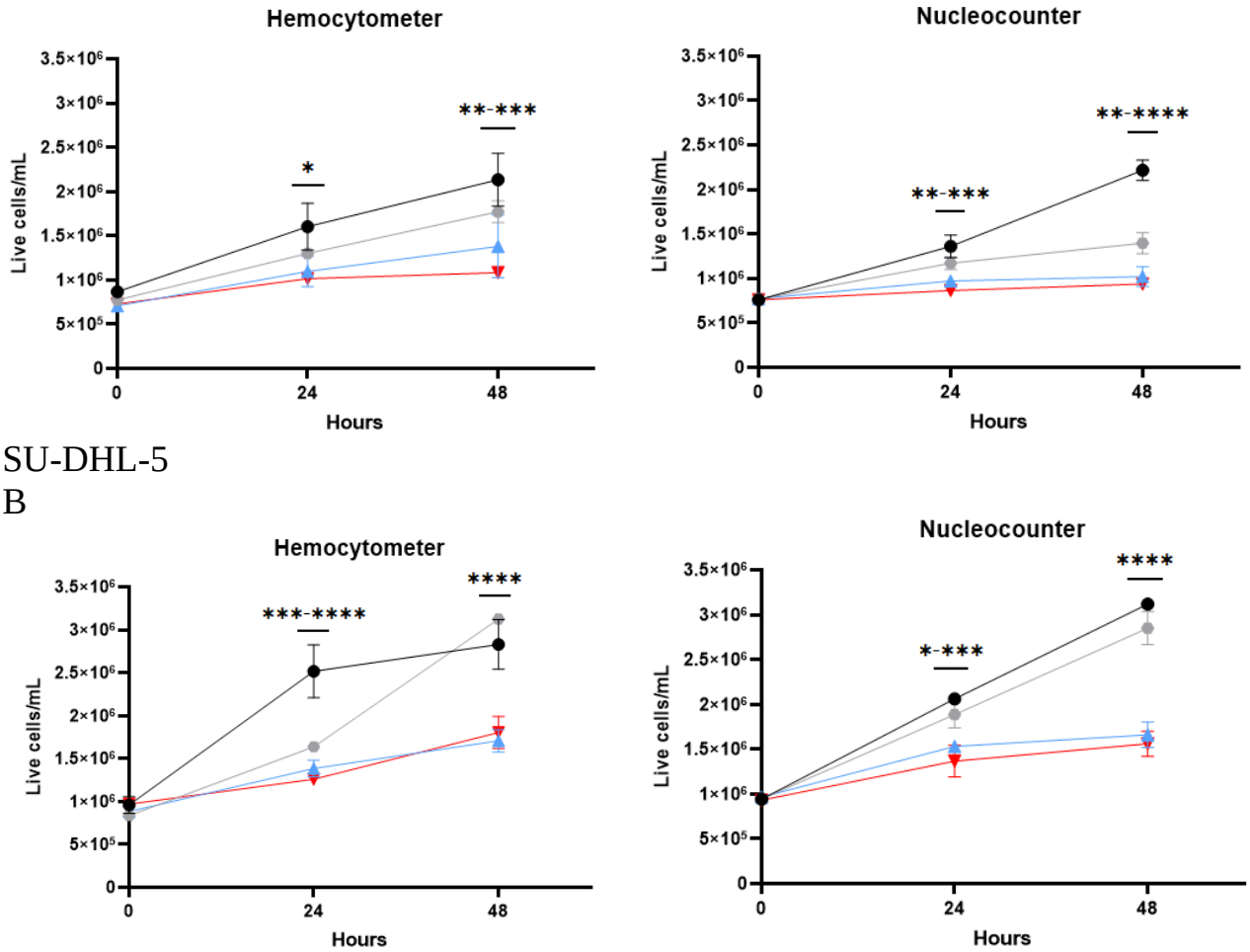

Figure 13: Cell viability assay of RIVA (**A**) and SU-DHL-5 (**B**) after treatment with cisplatin and 17AAG as single drugs and in combination for 0, 24 and 48 hours, along with vehicle controls. Live cells presented in both replicates of each sample were counted with trypan blue exclusion assay on hemocytometer. The cell count was further validated with a nucleocounter. Two-way ANOVA with multiple comparisons between samples at each timepoint was used for statistical analysis. Significant differences are showed with: *p value≤ 0.05, ** p value≤ 0.01, *** p value≤ 0.001, and **** p value≤ 0.0001.

5.5 The protein expressions of DDR proteins were affected by 17AAG exposure

Quantitative proteome analysis was performed on RIVA and SU-DHL-5 cells that were treated with cisplatin and 17AAG as single drugs and in combination for 0, 24 and 48 hours, along with vehicle controls. The SU-DHL-5 samples treated with cisplatin and combination for 0 hours were lost in the sample preparation for the proteome analysis and could therefore not be included. Each timepoint was prepared in single biological replicate and analytical duplicates.

The main goal of quantitative proteome analysis is to investigate the global protein expression in cells which was initially investigated with an unsupervised Principal Component Analysis (PCA) (Figure

14) to identify and visualize the variance between all RIVA and SU-DHL-5 samples included in the quantitative proteome analysis. The PCA presents a two-dimensional plot, with one component on each axis where each proteomic dataset of single LC-MS/MS analysis is represented by a single data point in the scores plot and individual gene identifiers distributed in the corresponding loading plot. The two components are based on the maximal variances of the protein quantification in all samples, where component 1 accounts for 55.6% of the variance whereas component 2 accounts for 9.5% of the variance. Each dot in the PCA shows an average proteome quantification data of the duplicates of each sample and the dots cluster in a cell line specific manner on the x-axis showing that the main protein variances between the analyzed samples constituting component 1 is between the cell lines (Figure 14). In addition, the data points show a relative clustering according to drug exposure time on the y-axis, indicating that the second main variance, constituting component 2, is based on the timepoints (Figure 14).

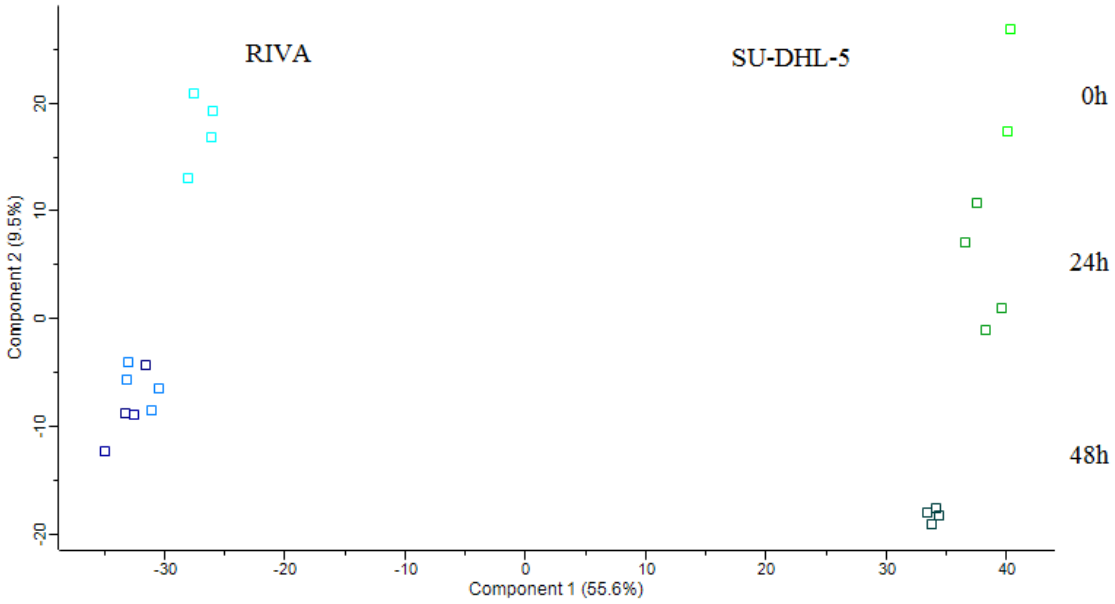

Figure 14: Principal component analysis (PCA) of all samples included in the quantitative proteome analysis presenting the protein variances between the samples. The two components are based on the maximal variances in the protein quantification. Each dot present protein quantification data of one sample based on average of its duplicates. The samples cluster according to their cell line categorization on x-axis (component 1) and are colored with blue (RIVA) and green (SU-DHL-5). On the y-axis (component 2) the samples cluster relatively together according to timepoints, presented with darker colors for longer time exposure.

The drug exposure experiments of the samples analyzed for quantitative proteomics were conducted in biological singlets and in technical duplicates of each sample which constituted insufficient number of replicates to perform a statistical comparison between the global protein expression profile of the

different treatment samples and vehicle controls. Therefore, a pilot study with more targeted protein expression analysis was performed. The thesis focused on DDR related proteins based on their involvement in cisplatin response and resistance. Moreover, 17AAG induces its synergistic effects with cisplatin possibly through effect on DDR, contributing to further relevance of gaining insight to the DDR system.

Cisplatin induced DNA damage is repaired mainly through the Nucleotide excision repair (NER) and DNA mismatch repair (MMR) pathways of the DDR system and therefore the core NER and MMR proteins [51] were analyzed. The core NER proteins are CUL5, ERCC1, ERCC2, ERCC4, ERCC5, ERCC6, POLE, POLE3, XPA, and XPC whereas the core MMR proteins constitute EXO1, MLH1, MLH3, MSH2, MSH3, MSH6, PMS1, and PMS2. Five of the core NER proteins were not detected in the quantitative proteome analysis and further three proteins had invalid protein expression values in both technical replicates of at least one sample and were therefore excluded. Remaining core NER (CUL5, ERCC2, ERCC5, POLE, POLE3 and XPC) and MMR proteins (MLH1, MSH2, MSH3 and MSH6) were extracted from the quantitative proteome data (Suppl. Figure 11). The genes encoding these proteins were not mutated in the two cell lines used for the experiments. The main purpose of this exploratory investigation was to examine the expression of these proteins after treatment with cisplatin and/or 17AAG, compared to vehicle control and therefore delta (Δ) values presenting quantitative differences between drug treatment and vehicle control were plotted (Figure 15). To calculate the Δ-values for each protein, the average LFQ values of the duplicates of drug treated samples was subtracted from average LFQ values of corresponding vehicle controls. Therefore, delta values above 0 show increased expression and values below 0 decreased expression of the proteins after drug treatment, compared to corresponding vehicle. Statistical analysis was not performed throughout the protein differential analysis as this is a pilot study with the purpose of gain insight into the tendencies seen for NER and MMR protein expression after cisplatin and/or 17AAG treatment.

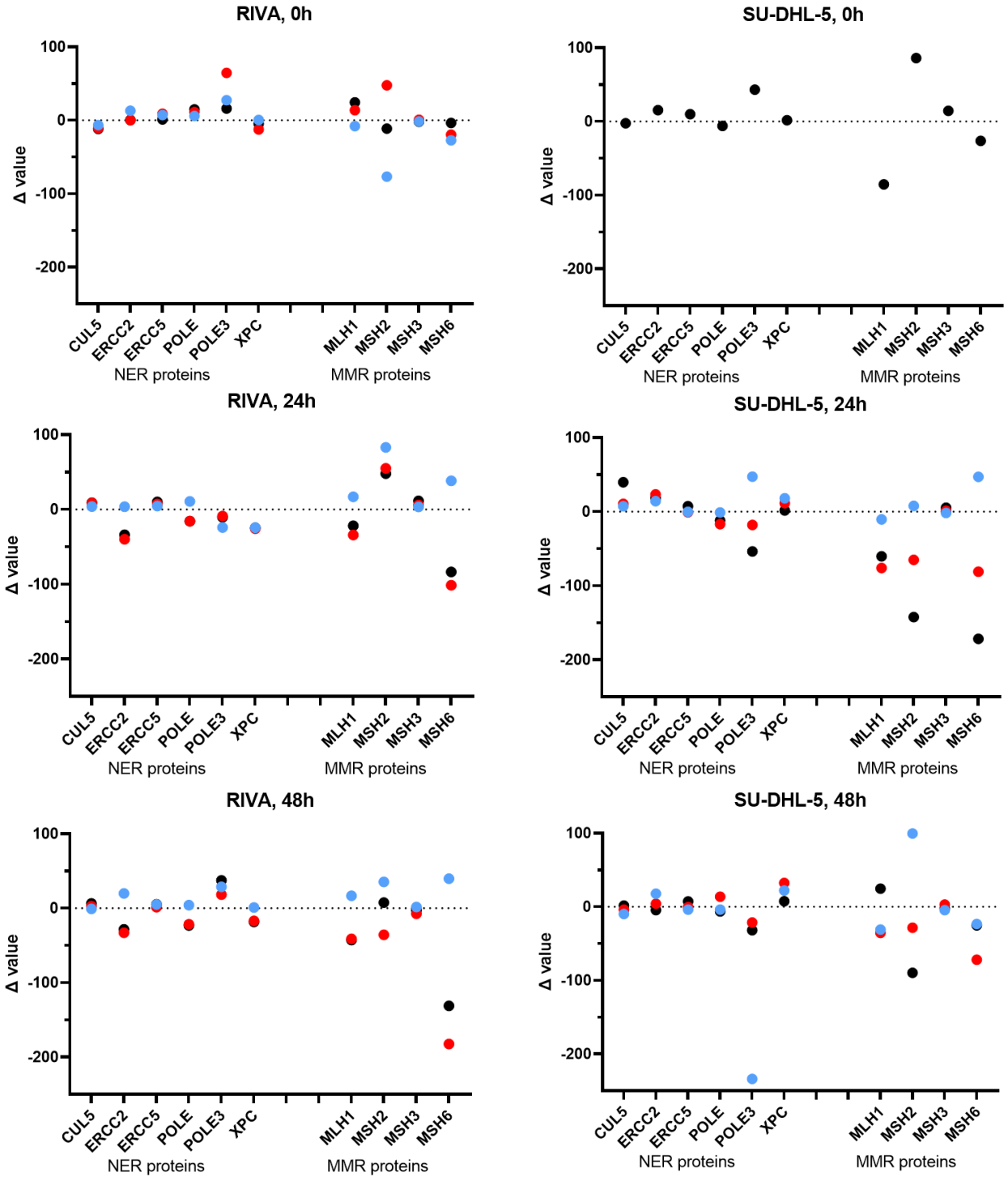

Figure 15: Differences of the quantitative protein values of each NER or MMR protein between the drug treatments and vehicle control presented with delta (Δ) values for each time point in RIVA and SU-DHL-5 cell lines. The Δ values were calculated by subtracting the average LFQ data of the duplicates of the drug treated samples from the average LFQ data of the duplicates of the vehicle controls. SU-DHL-5 cells treated with cisplatin and combination of cisplatin and 17AAG for 0 hours were excluded due to methodological issues. No statistical analysis was performed.

For both SU-DHL-5 and RIVA cells, MSH2 and MSH6 showed the highest variances between the Δ-values of drug and vehicle treatments (Figure 15) and were therefore further investigated for Δ-values throughout time (Figure 16). MSH2 and MSH6 are an essential part of the MMR pathway in the DDR system, and act together as a dimer termed MutSα to identify DNA damage in form of DNA mispairs and short insertion and deletion loops and subsequently initiate the MMR response [93]. In the conducted analysis increased expression of both proteins, with Δ-values above 0, was observed in cisplatin single drug treated RIVA and SU-DHL-5 cells for 24 hours, compared to corresponding vehicle control (Figure 16A-D). This can possibly be due to increased dsDNA damage after cisplatin exposure that activates DDR response leading to increased expression of MMR proteins. In agreement, a two-fold change of the Δ-value for both proteins in RIVA cells treated with cisplatin single drug for 24 hours was observed compared to cisplatin treatment for 0 hours (Figure 16A and C). After 48 hours of cisplatin single drug treatment, MSH2 still had higher expression compared to vehicle control in both RIVA and SU-DHL-5 cells (Δ-value above 0) (Figure 16A-B). MSH6 showed same tendencies as MSH2 after cisplatin single drug exposure with an outlier in SU-DHL-5 cells after 48-hour exposure. (Figure 16C-D).

In contrast, combining cisplatin with 17AAG resulted in a decrease of MSH2 and MSH6 protein expression with all Δ-values below 0, except for 0- and 24-hour RIVA samples showing slight increase in MSH2 expression (Figure 16A-D). Thus, the increased expression of MSH2 and MSH6 after cisplatin treatment was diminished and reversed by the addition of 17AAG in both RIVA and SU-DHL-5 cells. Same decreasing effect tendencies for both proteins were seen for 17AAG single drug, suggesting the possibility that 17AAG leads to degradation of DDR proteins through inhibition of Hsp90 chaperoning functions.

Briefly, the results showed that expression of both MSH2 and MSH6 were increased by cisplatin treatment opposed to the addition of 17AAG to cisplatin and by 17AAG single drug where decreased expression was observed. Thus, supporting that 17AAG has inhibitory effect on the expression of the two MMR proteins.

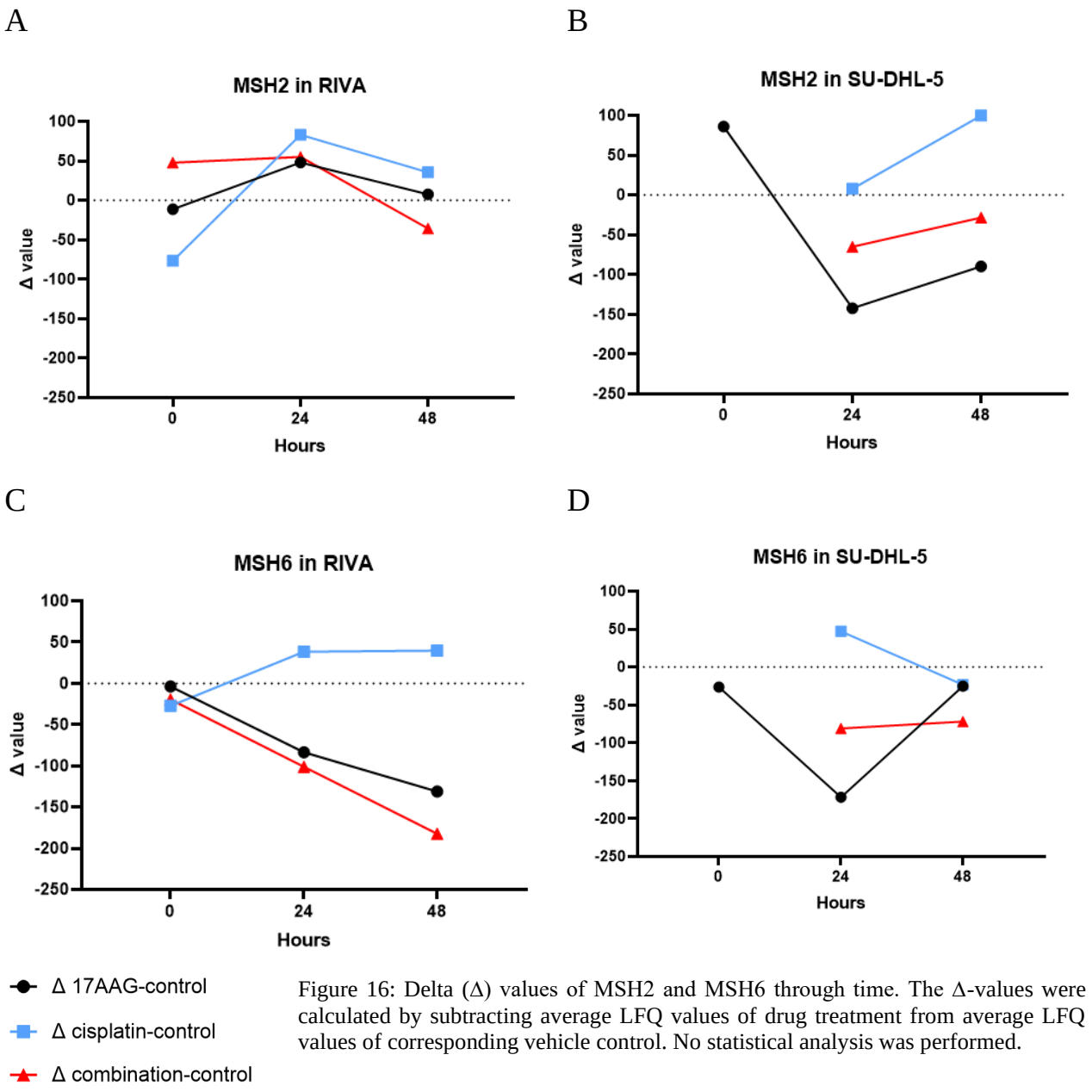

Figure 16: Delta (Δ) values of MSH2 and MSH6 through time. The Δ-values were calculated by subtracting average LFQ values of drug treatment from average LFQ values of corresponding vehicle control. No statistical analysis was performed.

The molecular activity and function of MSH2 and MSH6 were investigated further with the string database (string-db.org). Through this database it is possible to search for multiple proteins together at once and find interactions and common molecular function and biological processes of the proteins (Suppl. Figure 12). Besides working together as an essential part of the MMR the results from the string search showed that they are involved in the intrinsic apoptotic signaling pathway in response to DNA damage. This can possibly explain the tendency of MSH2 in RIVA and SU-DHL-5 cells where the increased expression of MSH2 was seen after 24 hours of drug treatment (Figure 16A-B) which can be the result of MSH2 reacting with DNA damage. However, when RIVA cells had been treated for 48 hours MSH2 expression was decreased (Figure 16A) which could be the cause of the

apoptotic effect of MSH2, leaving fewer cells with DNA damage left and thereby decreased need of MMR proteins. Interestingly, the string analysis also showed that MSH2 and MSH6 are involved in somatic hypermutation of immunoglobulin genes and isotype switching which suggests their importance of generating MMR in B-cells to maintain genome stability. Lastly, the string analysis showed that MSH2 and MSH6 are involved in platinum resistance, meaning that they are involved in determining the cells response to cisplatin. However, it could not be anticipated by the string analysis if increased or decreased expression of the proteins contribute to the resistance.

The Hsp90 proteins were also of interest in the quantitative proteome analysis because of 17AAG's effect on Hsp90, inhibiting its chaperoning effect [71]. Hsp90 proteins are molecular chaperones that have two human isoforms, namely Hsp90 alpha (HSP90AA1) and Hsp90 beta (HSP90AB1). Similar to MSH2 and MSH6, the two isoforms of the Hsp90 protein were investigated for differences between drug treatment and corresponding control presented with Δ-values at each time point for both cell lines (Figure 17). Hsp90 is very abundant and highly conserved, accounting for 1-2% of all proteins in most cells [94] and even more in malignant cells [95]. Accordingly, the y-axis shows large numbers with a wide range of Δ-values.

HSP90AA1 expression after cisplatin single drug treatment showed levels similar to the corresponding controls with Δ-values approximately at zero at all timepoints for both cell lines (Figure 17A-B). The HSP90AB1 isotype showed however some variations in expression after cisplatin treatment with no apparent pattern. It decreased slightly after 24 hours but then increased after 48 hours in RIVA (Figure 17C). However, HSP90AB1 showed steady expression through time in SU-DHL-5 with slightly higher expression in cisplatin alone treatment, compared to vehicle control (Figure 17D). According to the various expressions of the proteins after cisplatin treatment, cisplatin has not been suggested to have any effect on the Hsp90 chaperone protein, opposed to 17AAG known to prevent Hsp90 chaperone's function by inhibiting the formation of the Hsp90 complex.

Increased expression of both Hsp90 isoforms was observed in RIVA cells treated with 17AAG as single drug and in combination with cisplatin in a time-dependent manner (Figure 17A and C). This is presumably based on that 17AAG inhibits the formation and function of the Hsp90 complex and consequently the cell attempts to compensate for the loss of Hsp90's effect by accelerating the translation of Hsp90 proteins. In agreement, SU-DHL-5 cells treated with 17AAG as single drug and in combination with cisplatin for 24 hours showed higher expression of both HSP90AA1 and HSP90AB1 compared to corresponding controls (Figure 17B and D). However, after 48 hours of

exposure the increased expressions of both Hsp90 isoforms were decreased to levels similar to corresponding controls (Figure 17B and D). Possible explanation hereof is that the drug exposure leads to diminished cell viability where the apoptotic process of the cells ensues degeneration of all cell components, including Hsp90. This is supported by the cell viability assay presented before where combinatory drug exposed SU-DHL-5 cells showed significantly lower cell viability after 24 and 48 hours.

Summarily, by exposing DLBCL cell lines to the Hsp90 inhibitor 17AAG, expressions of both isoforms of the Hsp90 protein were highly increased in both cell lines after 24 hours suggested to be the cellular response of the inhibitory effect on Hsp90's function.

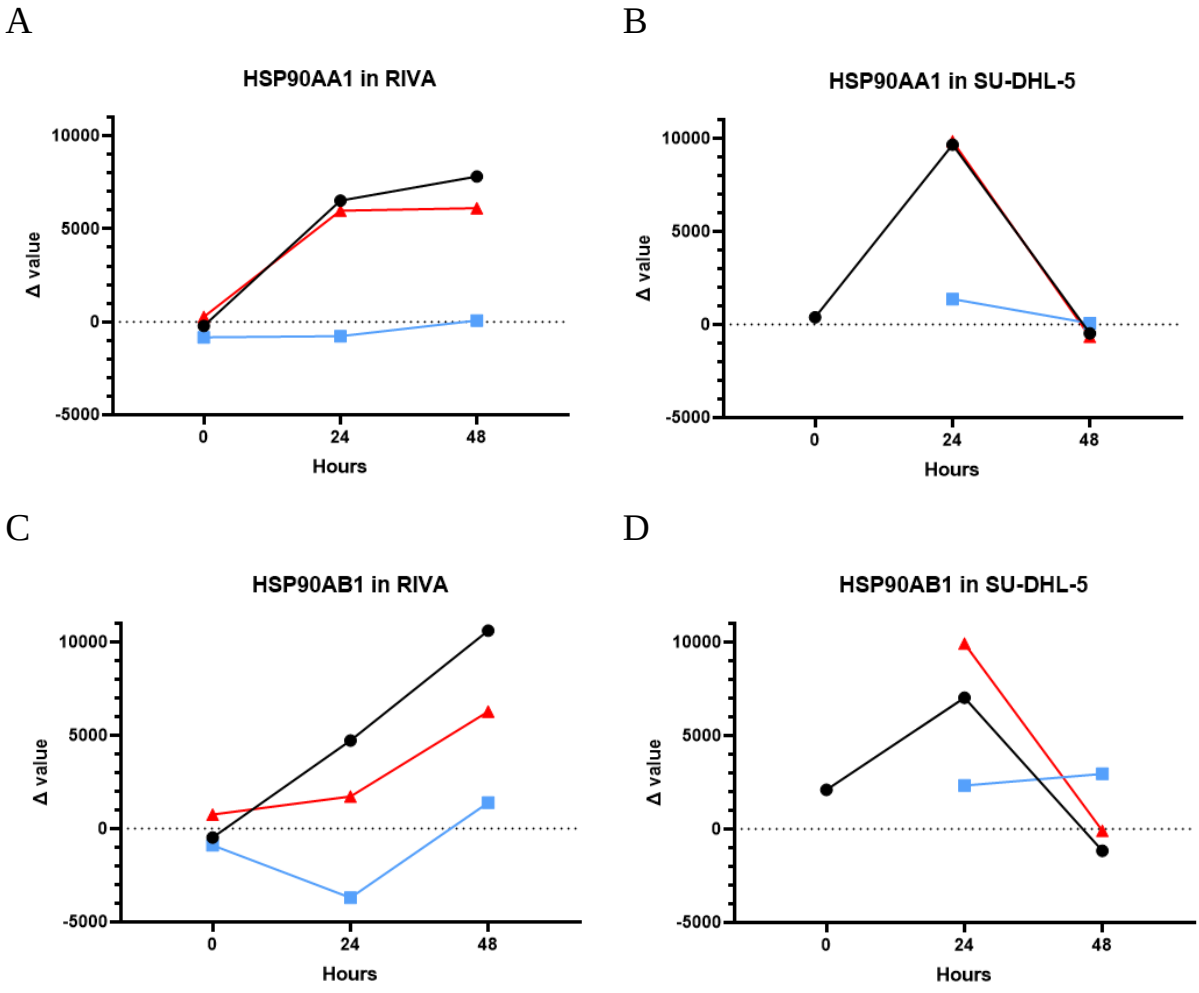

Figure 17: The two human isoforms of Hsp90 protein, HSP90AA1 and HSP90AB1, were investigated for protein expression after treatment with vehicle, cisplatin, 17AAG and a combination. The difference of duplicate average of drug treatment and vehicle treatment at each timepoint are presented with delta (Δ) values. The y-axis constitutes high numbers due to the abundancy of Hsp90 in malignant cells. No statistical analysis was performed.

6. Discussion

This thesis investigated if 17AAG can sensitize DLBCL cells to cisplatin. This was pursued by treating two DLBCL cell lines, RIVA and SU-DHL-5, with cisplatin and 17AAG as single drugs and in combination, along with corresponding controls. This was followed by examining the effect of each treatment parameter on DNA damage, cell cycle function, apoptosis activity, cell viability and differential protein expression of DDR related proteins. The following discussion will firstly address the results of this thesis, secondly limitations that have arisen through the experimental course and lastly future perspectives.

6.1 dsDNA damage measured with anti-γH2AX staining

The DNA damage analysis was conducted by staining RIVA and SU-DHL-5 cells with the dsDNA damage marker, anti-γH2AX, followed by flow cytometry assay. RIVA showed high levels (percentage of γH2AX+ cells) of dsDNA damage after treatment with cisplatin alone and in combination with 17AAG for 24 and 48 hours. More interestingly, significantly more dsDNA damage after combination treatment was observed compared to cisplatin alone when the mean intensities of γH2AX+ were compared based on the fluorescent intensity γH2AX histogram. This shows a synergistic cytotoxic effect of cisplatin and 17AAG in form of dsDNA damage induction in RIVA, which is in agreement with our previous results [72]. In contrast, SU-DHL-5 had highest levels of dsDNA damage after cisplatin alone after 24 and 48 hours. The documented increase in phosphorylated H2AX in cisplatin treated cells is however, a well-known concept that is already described in other studies [96,97]. Therefore, investigating if the DNA damage effect of cisplatin can be enhanced by adding 17AAG and if it can support the synergism of DLBCL cells observed with MTS assays in previous results [72] was of most interest. However, SU-DHL-5 does not obtain any enhanced DNA damaging effect by combination treatment, suggesting that cisplatin alone induces the maximal DNA damaging effect and therefore the documented synergism of the two drugs can possibly be based on other cellular processes than induction of DNA damage in SU-DHL-5. This is in contrast with RIVA cells which show that a synergistic effect is induced by addition of 17AAG indicating that the enhanced DNA damaging effect of 17AAG addition is a cell-specific effect in resistant cell lines. This presents a translational problem since some DLBCL patients might not benefit from the addition of 17AAG in regard to DNA damaging effect. On the other hand, the resistant cell-specific effects could be an interesting take on developing more personalized therapy where the cell-specific effects can be exploited as therapeutic strategy of DLBCL patients that

exhibits insensitive response to cisplatin. However, this thesis only included two cell lines, one sensitive and one resistant. Thus, to support the cell-specific effects of 17AAG addition to cisplatin, analogous experiments to this thesis should be repeated in more cell lines. In relation to this, the categorization of the two cell lines as sensitive and resistant should be carefully noted as it is based on the response of each cell line in relation to the other cell lines. On this basis, the categorization is very dependent on which cell lines are compared for cisplatin response, how many cell lines are included and how the cut-off between sensitive and resistant cell lines is defined. Thus, the RIVA cell line is not an absolutely resistant cell line but relatively more resistant than SU-DHL-5.

Noticeably, the fluorescent intensity γH2AX histograms for both cell lines showed that the vehicle control has a higher intensity than the unstained sample, showing H2AX phosphorylation without cisplatin induced DNA damage. An immunohistochemical study by Derenzini et al. [98] investigated the γH2AX expression in 99 DLBCL patient tumor samples where constitutive γH2AX expression where present in 47% of cases which is also in agreement with the theory of DLBCL tumors having high levels of genomic instability [54]. The present study is not fully comparable with those findings as DLBCL cell lines are used rather than patient tumor samples. However, the results from Derenzini's study suggests a constitutive H2AX phosphorylation in DLBCL cells. We still wanted to test this theory, so we performed an analogous dsDNA damage analysis with anti-γH2AX staining on Human Embryonic Kidney 293 (HEK) cells to investigate the baseline γH2AX expression in untreated HEK cells and compare them to untreated B-cells. The results hereof showed that the untreated HEK cells had higher intensity of anti-γH2AX compared to a corresponding unstained sample and lower intensity compared to the untreated RIVA and SU-DHL-5 cells, suggesting a cell specific baseline phosphorylation of H2AX (Suppl. Figure 13). In accordance, the fluorescent intensity histograms of RIVA and SU-DHL-5 show not a single peak but a high positive peak with a left-sided tail (Suppl. Figure 5-6). The tail is presumably not the result of a background signal as the antibody had been tested for the highest staining index and can therefore be considered as the population that only constitute the baseline H2AX phosphorylation in agreement with the constitute H2AX phosphorylation in B-cells theory.

6.2 Cisplatin disruption of the cell cycle distribution

The results from the cell cycle analysis through PI staining showed that cisplatin highly disrupts the cell cycle distribution in both cell lines. The PI staining of the cisplatin treated cells showed a clear G1-phase intensity peak followed by a wide peak presumably containing S- and G2/M-phases that

were hard to distinguish, implying that cisplatin blocks cells in post-G1 phases. This is in accordance with Velma et. al that showed accumulation of cells in S-phase after 1-3 µM cisplatin treatment for 24 and 48 hours using human promyelocytic leukemia cells [99]. Furthermore, another study states that increased duration of S-phase as well as a blockage in G2-phase is seen in cisplatin treated murine leukemia L1210 cells [100,101]. However, cisplatin is not described as cell cycle specific agent and as such, cisplatin can induce its DNA damaging effect in all proliferative cells regardless of the cell cycle phase state [100,102]. The disruption of the cell cycle was more prominent in RIVA cells causing the algorithm of the univariate cell cycle model to be unable to recognize the G1-, S-, and G2/M-phases in all cisplatin exposed cells. Consequently, the cell cycle phases were defined manually resulting in uncertain values of the distribution of the phases. To circumvent this problem, BrdU staining can be applied in combination with PI staining. BrdU is a synthetic nucleoside which can bind to DNA in replicating cells during S-phase and by combining it to the nucleic acid stain PI the resulting graphs contain both all DNA contents from PI staining and defined S-phase DNA from BrdU staining. This simplifies the separation of S-phase from the G1- and G2/M-phases with effortless characterization of the cell cycle phases in cisplatin treated cells [103,104]. Furthermore, G2/M cell cycle phase can also be pinpointed by the antibody against phosphorylated Histone 3 that is present during mitosis [105]. Other total DNA staining markers than PI also exists such as 7-AAD [105] and DRAQ5 [106] which in addition are not dependent on fixating the cell samples and can be used in living cells [105].

6.3 Apoptosis and cell viability after cisplatin and combination treatment

The apoptotic analysis showed high synergistic effect of cisplatin and 17AAG in RIVA cells with seven-fold increase in apoptotic cells compared to control after 48 hours of exposure which is in accordance with our previous results [72]. Contrarily, SU-DHL-5 showed no synergistic effects of combining cisplatin and 17AAG and generally smaller increase in apoptotic response after drug exposure compared to RIVA, however, SU-DHL-5 showed high number of early apoptotic cells in untreated cells, both at all 0-hour baseline samples and vehicle controls after 24 and 48 hours. This suggests a baseline activation of apoptotic processes in the SU-DHL-5 cell line which can be supported with a study by Abbott et al. showing that SU-DHL-5 cell line does not express the anti-apoptotic regulator protein BCL-2 which suggests that baseline SU-DHL-5 lacks the ability to prevent apoptosis resulting in high baseline pro-apoptotic levels [107]. It was unknown if untreated SU-DHL-5 cells can reverse the pro-apoptotic process and inhibit early apoptotic cells to terminate the apoptosis. This was investigated with cell viability analysis where both cell lines were counted for

total cells and live cells after 0, 24 and 48 hours after drug exposure, along with vehicle controls. Here, all 0-hour SU-DHL-5 samples show a slightly higher cell viability than all 0-hour RIVA samples, with approximately one million live cells/mL which shows that the high amount of early apoptotic SU-DHL-5 cells present cells that are metabolic active. Through time, the SU-DHL-5 vehicle controls show increased cell viability with significantly higher number of metabolic active cells compared to the SU-DHL-5 cells treated with cisplatin and combination. This supports that the early apoptotic SU-DHL-5 cells are able to reverse the pro-apoptotic process and survive. The cell viability through time in RIVA cells show that the combination of cisplatin and 17AAG decreases the cell viability exhibiting the lowest number of metabolic active cells, most prominent after 48 hours counted on the hemocytometer. This is in agreement with a study revealing lowered cell viability after treatment with cisplatin in combination with a Hsp90 inhibitor in ovarian as well as head and neck cancer cells [108,109].

Collectively, the overall effects of combining cisplatin with 17AAG on phenotypic cellular mechanisms is induction of dsDNA damage that causes cell cycle arrest which leads to disruption of the cell cycle distribution that can activate apoptosis of the treated cells resulting in decreased cell viability. Interestingly, a markedly enhanced effect on dsDNA damage and apoptosis was observed in combination treated RIVA cells, compared to treatment with cisplatin alone.

6.4 Differential protein expression of DDR related proteins

To test the potential and experimental set up with drug exposed cell lines a pilot assay for differential protein expression analysis was performed on DDR related proteins. The purpose was to strengthen our results showing synergistic effects of the combining cisplatin with 17AAG in RIVA by supporting that it is caused by impaired DDR likely through degradation as Hsp90 clients. This was performed with quantitative proteome analysis which, as stated previously, is a global proteome experimental method that we could not fully exploit because of lack of replicates. Instead, we performed a targeted core NER and MER protein expression analysis with extracted LFQ values from the quantitative analysis.

From the NER and MMR proteins investigated, MSH2 and MSH6 exhibited the highest differences between the drug treatments and vehicle control and were investigated further through time (0, 24 and 48 hours). For more extensive analysis, 96-hour timepoint could have been relevant to add anticipating that for cells to identify, signal, and have effect on protein translation can take over 48 hours. 17AAG treatment as single drug and in combination with cisplatin showed decreasing effect

of the expression of MSH2 in SU-DHL-5 after both 24 and 48 hours of exposure, though it should be noted that none of the changes observed were significant. In agreement, downregulation of MSH2 by 17AAG in combination with the cytotoxic drug pemetrexed have been showed in non-small cell lung carcinoma cells [110]. In contrast, RIVA show increased expression of MSH2 after 24 hours of cisplatin, 17AAG and combination treatment compared to vehicle control with slight decrease after 48 hours. The MSH6 expression in both RIVA and SU-DHL-5 cells were decreased after 17AAG and combination treatment in a time-dependent manner for RIVA. Overall, 17AAG treatment shows decreasing effect of MSH2 and MSH6 both as a single drug and in combination with cisplatin, except for MSH2 in RIVA. This supports the theory of that 17AAG can lead to degradation of DDR proteins and in that way enhance the antitumor effects of cisplatin. Furthermore, MSH2 and MSH6 were found to have biological function involved in platinum resistance which is in accordance with a study using CRISPR screen that finds MSH2 to be one of the main genes mediating resistance towards cisplatin in muscle invasive bladder cancer cells [111]. Accordingly, MSH2 and MSH6 constitute interesting players in cisplatin response that would be valuable to investigate further.

The two human isoforms of the Hsp90 protein, HSP90AA1 and HSP90AB1 were also investigated for protein expression through time after treatment with cisplatin, 17AAG and combination, along with vehicle control. Although Hsp90 inhibitor combined with DNA damaging agents such as cisplatin is a well-developed concept [112,113], there is limited research demonstrating the effect of the inhibitors on expression of Hsp90 isoforms on mRNA and protein level. This thesis' results show that both isoforms have clearly higher expression in 17AAG, and combination treated RIVA cells compared to corresponding controls. SU-DHL-5 cells also show high expression of 17AAG exposed cells both as single drug and in combination with cisplatin for 24 hours, however, after 48 hours the expression is decreased to the same level as the corresponding controls. This is in accordance with the cellular effect of the combination in SU-DHL-5 showing the levels of dsDNA damage and apoptosis to peak at 24 hours with decreased effect after 48 hours. Possible explanation hereof is that drug exposed SU-DHL-5 cells are eliminated fast and therefore after 48 hours there are fewer drug exposed cells that present drug effects.

For future proteome experiments we will conduct the analysis with more replicates of the cell line samples or preferably clinical patient samples of rrDLBCL cases that would enable us to get a wide picture of the whole-proteome expression. This includes all DDR related proteins after cisplatin and/or 17AAG treatment where the most significant differentially expressed DDR proteins can be validated with ELISA or Western Blot and investigated further on genetic base by performing ddPCR.

6.5 Limitations

The main limitation of this thesis is related to the chosen cisplatin-sensitizing drug, 17AAG. The essence of combining 17AAG with cisplatin to plausibly enhance the antitumor effects of cisplatin is based on 17AAGs inhibitory effect on DDR [70,71]. The inhibition is however gained indirectly through binding to the Hsp90 chaperone binding site, blocking its ability to bind and activate its clients, which leads to degradation of the clients, including DDR [70,71]. However, Hsp90 has more than 200 clients involved in neuronal signaling, immune response, angiogenesis, cytokine signaling, DDR, and many other processes [114] and therefore the Hsp90 inhibitory effect of 17AAG is not specific to the DDR system [71,115]. Therefore, we cannot reject the possibility that the synergism of cisplatin and 17AAG are based on other cellular processes than DDR. Additionally, 17AAG has not been approved for use in the clinic yet. Therefore already approved agents, like the Hsp90 inhibitor PU-H71 (currently under first-in-human phase I trial [116]), could have been more relevant in term of clinical relevance. Moreover, with focus on DDR, agents that directly inhibit targeted DDR proteins is an interesting application to investigate the direct effect of DDR on cisplatin response and if cells can be sensitized through explicit inhibition of DDR components. This has been tested in ovarian cancer cells where ERCC1, an important component of the NER pathway of the DDR system, was inhibited revealing sensitizing effects to cisplatin [117]. However, cisplatin-induced DNA damage can activate different DDR pathways involving a wide range of DDR related proteins [50] and therefore direct inhibitory of targeted DDR proteins in specific pathways can presumably not be sufficient to inhibit all DDR activity involved in cisplatin-induced DNA damage. In this matter, the degradation of Hsp90 clients including various DDR proteins through effect of 17AAG potentially results in wider DDR inhibitory effect. This effect is very attractive for treatment of tumors showing resistance towards cisplatin as the resistance mechanism can involve wide range of dysfunctional DDR components that through the DDR system can repair the cisplatin-induced dsDNA damage. This is in accordance with the results of this thesis showing 17AAG sensitizing RIVA to cisplatin which based on previous dose response screens [72] have been categorized as resistant to cisplatin.

Additional limitation was that the anti-γH2AX antibody, used to detect cisplatin-induced dsDNA damage is not completely specific to DNA damage caused by cisplatin. A positive γH2AX fluorescent signal can also be the result of the pan-nuclear phosphorylation of H2AX due to DNA fragmentation involved in apoptosis as stated previously in this thesis. Despite that this confounding factor was eliminated by observing γH2AX signal short time after exposure (4 and 8 hours) prior to apoptosis

(Suppl. Figure 3-4), other dsDNA damage markers than H2AX could be included to help distinguish the effect of cisplatin and general apoptosis. One candidate is the tumor suppressor P53-binding protein 1 (53BP1) which is one of the key players in dsDNA damage responses as it is recruited to the damaged nuclear site and acts as a mediator of the DDR system [118]. This marker has been used to measure dsDNA damage in a variety of studies [119–121]. Another technical challenge is the fact that cisplatin does not exclusively induce dsDNA breaks as its binding to guanine on the DNA can result in mismatch and ssDNA breaks which γH2AX does not detect. Thus, to obtain a full overview of DNA damage, techniques like comet assay could have been applied which detects various DNA damage, such as ssDNA and dsDNA damage [122]. However, due to limited time and cost considerations these were not included. In essence, there are some considerations to take into account when using γH2AX as a measurement of cisplatin-induced dsDNA damage including specificity and selectivity, however, there is a general consensus that anti-γH2AX is a great marker for dsDNA damage and is still widely used for that purpose [83,84,123–126].

6.6 Future perspectives

In summary, the results of this thesis show that cisplatin induces dsDNA damage with high efficiency which results in cell cycle arrest with disrupted cell cycle distribution leading to DDR mediated apoptosis resulting in lower cell viability of the cisplatin affected cells. The combination of cisplatin and 17AAG showed synergistic effect on DNA damage, apoptosis, and cell viability for RIVA contrary to SU-DHL-5 showing no markedly enhanced effect. Furthermore, 17AAG as single drug and in combination with cisplatin generally decreases the MSH2 and MSH6 proteins involved in MMR and increases Hsp90 isoforms expression presumably caused by a compensatory effect due to Hsp90 inhibition, validating that the enhancing effect of adding 17AAG is based on its inhibitory effect on HSp90 and DDR proteins.

The documented synergistic effects in RIVA are interesting as the clinical purpose of adding 17AAG to cisplatin treatment is to gain better response in patients that normally show resistance towards cisplatin. Hence, the fact that RIVA is observed to be resistant towards cisplatin. However, further experiments on this matter are yet to be conducted to support the potentiality. Initially, tracking the effect of the combination compared to cisplatin alone on DNA damage, cell cycle, apoptosis and cell viability should be repeated in several more cisplatin resistant DLBCL cell lines where each treatment variable includes at least triplicates for stronger statistical analysis. Furthermore, additional

experiments on other cellular effects of the cisplatin and 17AAG combinatory treatment, such as CFSE staining which enables quantification of cellular division [127], could support this data further.

The involvement of DDR in both cisplatin resistance and the synergistic effects of combining cisplatin to 17AAG was only touched upon in this thesis with a pilot study observing tendencies of differential expression of NER and MMR proteins. Noteworthy, DDR inhibition constitutes a highly relevant and interesting add-on target to sensitize cells to cisplatin. As described previously, NER and MMR are the main DDR pathways activated during cisplatin-induced DNA damage. The two pathways work in very different ways where through NER the DDR system attempts to repair the DNA damage and sometimes is successful. Overexpressed NER components have increased success of repairing cisplatin-induced DNA damage and is therefore associated with cisplatin resistance [49]. Therefore, it is highly relevant to inhibit the NER pathway to overcome the resistance. In contrast, MMR attempts but is never successful of repairing the invasive cisplatin DNA adducts, consequently initiating apoptosis [50]. Inhibition of MMR is therefore not desired to sensitize cells to cisplatin. Targeting the different DDR pathways in different ways is therefore admissible. Additionally, it can be discussed that even though the DDR pathways have different roles in cisplatin's resistance and efficiency, wide DDR inhibition will most likely prevent all repair mechanism and although MMR is also inhibited the cell cannot survive with unrepaired invasive cisplatin-induced DNA damage and inhibiting DDR constitute therefore highly potential way to overcome cisplatin resistance. Furthermore, DDR constitute a particularly interesting target in DLBCL because the normal B-cell development is highly dependent on functional DDR as the cells are exposed to high levels of DNA damage due to the recombination of the Ig-gene segments and somatic hypermutation and class switch recombination in the germinal center. Therefore, using an agent that rules its effect by inhibiting DDR, such as 17AAG is highly compatible in DLBCL. However, further exploratory analysis of the mode of action of 17AAG are needed to ensure that its sensitizing abilities on B-cells is achieved through DDR inhibition. In essence, more details regarding the different DDR components' role in cisplatin response is warranted. In this relation, exploring the DDR pathways' role in cell lines that show sensitizing effect to cisplatin by addition of 17AAG in more details could be interesting. An example hereof is investigating if NER pathway components are overexpressed in RIVA and other cisplatin resistant cell lines and in that way elucidate if the combinatory synergistic effect is based on inhibition of NER or other DDR mechanism that attempts to repair the cisplatin DNA adducts. This can be conducted with targeted protein analysis through ELISA or Western blot techniques.

This thesis had a specific focus on cisplatin and the possibility of enhancing cisplatin's cytotoxic effect by addition of 17AAG. In the clinic, cisplatin is administered as a part of a regimen constituting numerous agents, namely R-DHAP (rituximab, dexamethasone, cytarabine/Ara C and cisplatin) and R-GDP (rituximab, gemcitabine, dexamethasone and cisplatin). Therefore, it could be interesting to investigate if the cisplatin and 17AAG synergistic effects are also seen when combined with the existing regiments. For further analysis, this should be investigated both on cellular level as well as in animal studies which additionally can assess adverse toxicity when combining 17AAG to the cisplatin containing regimens.

All in all, this thesis has demonstrated that by combining the Hsp90 inhibitor, 17AAG, with cisplatin, the cytotoxic effect on resistant DLBCL cells is enhanced. This elucidates high potentiality of sensitizing cisplatin resistant DLBCL patients to cisplatin, whereby the cisplatin resistance can be overcome. Thus, with further studies and implementation to the clinic, Hsp90-inhibitor add-on drug to cisplatin can guide the way to a new and better treatment option and outcome in rrDLBCL.

7. Conclusion

This thesis investigated if 17AAG can sensitize DLBCL cells to cisplatin by evaluating the combinatory effects of 17AAG and cisplatin in two DLBCL cell lines, RIVA and SU-DHL-5. Synergism was assessed on DNA damage, cell cycle distribution, and apoptosis activity, and analyzed by flow cytometry. Additionally, the cell viability and differential expression of DDR related proteins were investigated in the treated DLBCL cells.

Enhanced effect of dsDNA damage was observed after adding 17AAG to cisplatin treatment in RIVA cells, resulting in disruption of cell cycle progression and a more than three-fold increase in apoptosis in comparison to single-drug treatment. Thus, 17AAG enhances cisplatin's cytotoxic effects as measured on different cellular mechanisms in the cisplatin-resistant cell line, RIVA. In contrast, these findings could not be observed in SU-DHL-5, where the cells exhibited maximal effects on dsDNA damage after treatment with cisplatin alone resulting in disturbance of cell cycle distribution and no enhancing effect of adding 17AAG to cisplatin on apoptosis. The data implies that the synergism between cisplatin and 17AAG could be based on cellular processes, such as DDR, that are associated with cisplatin resistance as the synergistic effects are only observed in a resistant DLBCL cell line. This was further supported by differential DDR protein expression where 17AAG showed to have different effect on DDR, compared to cisplatin alone and control, suggesting that 17AAG does affect the DDR and the synergism is possibly based on that molecular action. In summary, this thesis concludes that 17AAG sensitizes cisplatin resistant DLBCL cells to cisplatin and can thus be a potential therapeutical strategy to overcome the resistance.

8. References

1. MacConmara M, Lederer JA. B cells. Crit Care Med. 2005;33:514–6.
2. Maity PC, Datta M, Nicolò A, Jumaa H. Isotype Specific Assembly of B Cell Antigen Receptors and Synergism With Chemokine Receptor CXCR4. Front Immunol. 2018;9(December):3–5.
3. Treanor B. B-cell receptor: From resting state to activate. Immunology. 2012;136(1):21–7.
4. Budeus B, De Reynoso SS, Przekopowitz M, Hoffmann D, Seifert M, Küppers R, et al. Complexity of the human memory B-cell compartment is determined by the versatility of clonal diversification in germinal centers. Proc Natl Acad Sci U S A. 2015;112(38):E5281–9.
5. Takatsu K. Cytokines involved in B-cell differentiation and their sites of action. Proc Soc Exp Biol Med. 1997;
6. Agger R, Claus N, Leslie G, Aasted B. Udviklingen af B-celler. In: Immunologi. 1st ed. København: Munksgaard; 2015. p. 195–9.
7. Perez-Andres M, Paiva B, Nieto WG, Caraux A, Schmitz A, Almeida J, et al. Human peripheral blood B-Cell compartments: A crossroad in B-cell traffic. Cytom Part B - Clin Cytom. 2010;78.
8. Agger R, Claus N, Leslie G, Aasted B. Dannelse af kimcentre. In: Immunologi. 1st ed. København: Munksgaard; 2015. p. 208–10.
9. Pilzecker B, Jacobs H. Mutating for good: DNA damage responses during somatic hypermutation. Front Immunol. 2019;10(MAR):1–13.
10. Agger R, Claus N, Leslie G, Aasted B. Gener, der koder for den konstante del af H- og L-kæder. In: Immunologi. 1st ed. København: Munksgaard; 2015. p. 142.
11. Basso K, Dalla-Favera R. Germinal centres and B cell lymphomagenesis. Nat Rev Immunol. 2015;15(3):172–84.
12. Küppers R. Mechanisms of B-cell lymphoma pathogenesis. Nat Rev Cancer. 2005;5(4):251–62.
13. Lymphoma [Internet]. American Cancer Society. 2021 [cited 2020 Mar 27]. Available from: https://www.cancer.org/cancer/lymphoma.html
14. Swerdlow SH, Campo E, Pileri SA, Harris NL, Stein H, Siebert R, et al. The 2016 revision of the World Health Organization classification of lymphoid neoplasms. blood J. 2016;127(20):453–62.
15. Wang JJ, Lei KF, Han F. Tumor microenvironment: Recent advances in various cancer treatments. Eur Rev Med Pharmacol Sci [Internet]. 2018;22(12):3855–64. Available from: https://pubmed.ncbi.nlm.nih.gov/29949179/
16. Baylin SB, Jones PA. Epigenetic determinants of cancer. Cold Spring Harb Perspect Biol. 2016;8(9):1–35.
17. Hanahan D, Weinberg RA. The Hallmarks of Cancer. 2000;107.
18. Hanahan D, Weinberg RA. Hallmarks of cancer: The next generation. Cell [Internet]. 2011;144(5):646–74. Available from: http://dx.doi.org/10.1016/j.cell.2011.02.013
19. Armitage JO, Gascoyne RD, Lunning MA, Cavalli F. Non-Hodgkin lymphoma. Lancet [Internet]. 2017;390(10091):298–310. Available from: http://dx.doi.org/10.1016/S0140-6736(16)32407-2
20. Shankland KR, Armitage JO, Hancock BW. Non-Hodgkin lymphoma. Lancet [Internet]. 2012;380(9844):848–57. Available from: http://dx.doi.org/10.1016/S0140-6736(12)60605-9

21. Statistik om non-Hodgkin lymfom [Internet]. Kræftens bekæmpelse. 2018. Available from: https://www.cancer.dk/non-hodgkin-lymfom-lymfekraeft/statistik-nonhodgkin-lymfom/

22. Li S, Young KH, Medeiros LJ. Diffuse large B-cell lymphoma. Pathology [Internet]. 2018;50(1):74–87. Available from: https://www.sciencedirect.com/science/article/pii/S0031302517304713?via%3Dihub#bib9

23. Marianne Steding-Jessen, Dromph K, Damslund L. Malignt Lymfom og CLL National årsrapport 2018. Den landsdækkende LYFO database. 2018;(december):1–109.

24. Dansk Lymfomgruppe (DLG). Diffust storcellet B-celle lymfom. 2019;1–40. Available from: www.dmcg.dk/kliniske-

25. Smith SD, Chen A, Spurgeon S, Okada C, Fan G, Dunlap J, et al. Diffuse large B-cell lymphoma in adults aged 75 years and older: A single institution analysis of cause-specific survival and prognostic factors. Ther Adv Hematol. 2013;4(6):349–53.

26. Martelli M, Ferreri AJM, Agostinelli C, Di Rocco A, Pfreundschuh M, Pileri SA. Diffuse large B-cell lymphoma. Crit Rev Oncol Hematol [Internet]. 2013;87(2):146–71. Available from: http://dx.doi.org/10.1016/j.critrevonc.2012.12.009

27. Gascoyne RD, Campo E, Jaffe ES, Chan W., Chan JKC, Rosenwald A, et al. Diffuse large B-cell lymphoma, NOS. In: Swerdlow SH, Campo E, Harris NL, Jaffe ES, Pileri SA, Stein H, et al., editors. WHO Classification of Tumours of Haematopoietic and Lymphoid Tissues. 4th ed. Lyon: WHO Press; 2017. p. 585.

28. Castillo JJ, Winer ES, Olszewski AJ. Sites of extranodal involvement are prognostic in patients with diffuse large B-cell lymphoma in the rituximab era: An analysis of the Surveillance, Epidemiology and End Results database. Am J Hematol. 2014;89(3):310–4.

29. Shipp M et al. A Predictive Model for Aggressive Non-Hodgkin's Lymphoma. N Engl J Med. 1993;329(1):21–6.

30. Ruppert AS, Dixon JG, Salles G, Wall A, Cunningham D, Poeschel V, et al. International prognostic indices in diffuse large B-cell lymphoma: A comparison of IPI, R-IPI, and NCCN-IPI. Blood. 2020;135(23):2041–8.

31. Sehn LH, Berry B, Chhanabhai M, Fitzgerald C, Gill K, Hoskins P, et al. The revised International Prognostic Index (R-IPI) is a better predictor of outcome than the standard IPI for patients with diffuse large B-cell lymphoma treated with R-CHOP. Blood. 2007;109(5):1857–61.

32. Zhou Z, Sehn LH, Rademaker AW, Gordon LI, LaCasce AS, Crosby-Thompson A, et al. An enhanced International Prognostic Index (NCCN-IPI) for patients with diffuse large B-cell lymphoma treated in the rituximab era. Blood. 2014;123(6):837–42.

33. Ziepert M, Hasenclever D, Kuhnt E, Glass B, Schmitz N, Pfreundschuh M, et al. Standard international prognostic index remains a valid predictor of outcome for patients with aggressive CD20+ B-cell lymphoma in the rituximab era. J Clin Oncol. 2010;28(14):2373–80.

34. Alizadeh AA, Elsen MB, Davis RE, Ma CL, Lossos IS, Rosenwald A, et al. Distinct types of diffuse large B-cell lymphoma identified by gene expression profiling. Nature [Internet]. 2000;403(6769):503–11. Available from: https://pubmed.ncbi.nlm.nih.gov/10676951/

35. Schmitz R, Wright GW, Huang DW, Johnson CA, Phelan JD, Wang JQ, et al. Genetics and Pathogenesis of Diffuse Large B-Cell Lymphoma. N Engl J Med. 2018;378(15):1396–407.

36. Chapuy B et al. Molecular Subtypes of Diffuse Large B-cell Lymphoma are Associated with Distinct Pathogenic Mechanisms and Outcomes. Physiol Behav. 2018;66(4):693–8.

37. Wright GW, Huang DW, Phelan JD, Coulibaly ZA, Roulland S, Young RM, et al. A Probabilistic Classification Tool for Genetic Subtypes of Diffuse Large B Cell Lymphoma with Therapeutic Implications. Cancer Cell [Internet]. 2020;37(4):551-568.e14. Available from: https://doi.org/10.1016/j.ccell.2020.03.015

38. Gascoyne RD, Campo E, Jaffe ES, Chan W., Chan JKC, Rosenwald A, et al. Diffuse large B-cell lymphoma, NOS. In: WHO Classification of Tumours of Haematopoietic and Lymphoid Tissues. 4th ed. Lyon; p. 291-.

39. Pasqualucci L. The Genetic Landscape of Diffuse Large B-Cell Lymphoma. 2015; Available from: https://www.clinicalkey.com/#!/content/playContent/1-s2.0-S0037196315000062?returnurl=https:%2F%2Flinkinghub.elsevier.com%2Fretrieve%2Fpii%2FS0037196315000062%3Fshowall%3Dtrue&referrer=https:%2F%2Fpubmed.ncbi.nlm.nih.gov%2F

40. Frontzek F, Lenz G. Novel insights into the pathogenesis of molecular subtypes of diffuse large B-cell lymphoma and their clinical implications. Taylor Fr Online [Internet]. 2019;12(11). Available from: https://doi-org.zorac.aub.aau.dk/10.1080/17512433.2019.1683447

41. Nowakowski GS, Czuczman MS. ABC, GCB, and Double-Hit Diffuse Large B-Cell Lymphoma: Does Subtype Make a Difference in Therapy Selection? Am Soc Clin Oncol Educ B. 2015;(35):e449–57.

42. Dybkær K, Bøgsted M, Falgreen S, Bødker JS, Kjeldsen MK, Schmitz A, et al. Diffuse large B-cell lymphoma classification system that associates normal B-cell subset phenotypes with prognosis. J Clin Oncol. 2015;33(12):1379–88.

43. Read J, Koff J, Nastoupil L, Williams J, Cohen J, Flowers CR. valuating cell-of-origin subtype methods for predicting diffuse large B-cell lymphoma survival: A meta-analysis of gene expression profiling and immunohistochemistry algorithms. 2014;14(6):460–7.

44. Ngo V, Young R, Schmitz R et al. Oncogenically active MYD88 mutations in human lymphoma. Nature [Internet]. 2012; Available from: https://www.nature.com/articles/nature09671#citeas

45. Baech J, Hansen SM, Lund PE, Soegaard P, Brown P de N, Haaber J, et al. Cumulative anthracycline exposure and risk of cardiotoxicity; a Danish nationwide cohort study of 2440 lymphoma patients treated with or without anthracyclines. Br J Haematol. 2018;183(5):717–26.

46. Sarkozy C, Sehn LH. Management of relapsed/refractory DLBCL. Best Pract Res Clin Haematol [Internet]. 2018;31(3):209–16. Available from: https://doi.org/10.1016/j.beha.2018.07.014

47. Crump M, Neelapu SS, Farooq U, Van Den Neste E, Kuruvilla J, Westin J, et al. Outcomes in refractory diffuse large B-cell lymphoma: Results from the international SCHOLAR-1 study. Blood. 2017;130(16):1800–8.

48. Dansk Lymfomgruppe (DLG). Retningslinjerfor diagnostik og behandling afDIFFUST STORCELLET B-CELLE LYMFOM (DLBCL). 2015; Available from: https://docplayer.dk/18319732-Retningslinjer-for-diagnostik-og-behandling-af-diffust-storcellet-b-celle-lymfom-dlbcl-dansk-lymfomgruppe-2015.html

49. Basu A, Krishnamurthy S. Cellular responses to cisplatin-induced DNA damage. J Nucleic Acids. 2010;2010.

50. Rocha CRR, Silva MM, Quinet A, Cabral-Neto JB, Menck CFM. DNA repair pathways and cisplatin resistance: An intimate relationship. Clinics. 2018;73(8):1–10.

51. Knijnenburg TA, Wang L, Zimmermann MT, Chambwe N, Gao GF, Cherniack AD, et al. Genomic and Molecular Landscape of DNA Damage Repair Deficiency across The Cancer Genome Atlas. Cell Rep. 2018;23(1):239-254.e6.

52. Takagi M. DNA damage response and hematological malignancy. Int J Hematol. 2017;106(3):345–56.

53. Skibola CF, Curry JD, Nieters A. Genetic susceptibility to lymphoma. Haematologica. 2007;92(7):960–9.

54. Lawrence MS, Stojanov P, Polak P, Kryukov G, Cibulskis K, Sivachenko A, et al. Mutational heterogeneity in cancer and the search for new cancer genes. NIH Public Access. 2013;23(1):1–7.

55. Abbosh PH, Plimack ER. Molecular and Clinical Insights into the Role and Significance of Mutated DNA Repair Genes in Bladder Cancer. Bl Cancer. 2018;4(1):9–18.

56. Chatterjee N, Walker GC. Mechanisms of DNA damage, repair and mutagenesis. Environ Mol Mutagen [Internet]. 2017;58(3):235–63. Available from: https://www.ncbi.nlm.nih.gov/pmc/articles/PMC5474181/

57. Cervelli T, Borghini A, Galli A, Andreassi MG. DNA damage and repair in atherosclerosis: Current insights and future perspectives. Int J Mol Sci. 2012;13(12):16929–44.

58. Krokan HE, Bjoras M. Chapter 06: Base Excision Repair. Cold Spring Harb Perspect Biol. 2013;5(4):a012583.

59. Hegde M, Hazra T, Mitra S. Early Steps in the DNA Base Excision/Single-Strand Interruption Repair Pathway in Mammalian Cells. Cell Res [Internet]. 2008;18(1):27–47. Available from: https://www.ncbi.nlm.nih.gov/pmc/articles/PMC3624763/pdf/nihms412728.pdf

60. Kutuzov MM, Belousova EA, Kurgina TA, Ukraintsev AA, Vasil'eva IA, Khodyreva SN, et al. The contribution of PARP1, PARP2 and poly(ADP-ribosyl)ation to base excision repair in the nucleosomal context. Sci Rep. 2021;11(1).

61. Fell VL, Schild-Poulter C. The Ku heterodimer: Function in DNA repair and beyond. Mutat Res - Rev Mutat Res [Internet]. 2015;763:15–29. Available from: http://dx.doi.org/10.1016/j.mrrev.2014.06.002

62. Curtin NJ. DNA repair dysregulation from cancer driver to therapeutic target. Nat Rev Cancer. 2012;12(12):801–17.

63. Mikhed Y, Görlach A, Knaus UG, Daiber A. Redox regulation of genome stability by effects on gene expression, epigenetic pathways and DNA damage/repair. Redox Biol [Internet]. 2015;5:275–89. Available from: http://dx.doi.org/10.1016/j.redox.2015.05.008

64. Holohan C, Van Schaeybroeck S, Longley DB, Johnston PG. Cancer drug resistance: An evolving paradigm. Nat Rev Cancer. 2013;13(10):714–26.

65. Gottesman MM. Mechanisms of Cancer Drug Resistance. Annu Rev Med. 2002;53(615–27).

66. Wang X, Zhang H, Chen X. Drug resistance and combating drug resistance in cancer. Cancer Drug Resist. 2019;2(2):141–60.

67. Arora S, Kothandapani A, Tillison K, Kalman-Maltese V, Patrick SM. Downregulation of XPF-ERCC1 enhances cisplatin efficacy in cancer cells. DNA Repair (Amst) [Internet]. 2010;9(7):745–53. Available from: http://dx.doi.org/10.1016/j.dnarep.2010.03.010

68. Aebi S, Kurdi-Haidar B, Gordon R, Cenni B, Zheng H, Fink D, et al. Loss of DNA mismatch repair in acquired resistance to cisplatin. Cancer Res. 1996;56(13):3087–90.

69. Drummond JT, Genschel J, Wolf E, Modrich P. DHFR/MSH3 amplification in methotrexate-resistant cells alters the hMutSα/hMutSβ ratio and reduces the efficiency of base-base mismatch repair. Proc Natl Acad Sci U S A. 1997;94(19):10144–9.

70. Pennisi R, Ascenzi P, di Masi A. Hsp90: A new player in DNA Repair? Biomolecules. 2015;5(4):2589–618.

71. Talaei S, Mellatyar H, Asadi A, Akbarzadeh A, Sheervalilou R, Zarghami N. Spotlight on 17-AAG as an Hsp90 inhibitor for molecular targeted cancer treatment. Chem Biol Drug Des. 2019;93(5):760–86.

72. Schmidt L, Issa II, Haraldsdóttir H, Hald JL, Schmitz A, Due H, et al. Hsp90 inhibition sensitizes DLBCL cells to cisplatin. Cancer Chemother Pharmacol [Internet]. 2022;(0123456789). Available from: https://doi.org/10.1007/s00280-022-04407-5

73. Segrè D, DeLuna A, Church GM, Kishony R. Modular epistasis in yeast metabolism. Nat Genet. 2005 Jan;37(1):77–83.

74. Bliss CI. The toxicity of poisons applied jointly. Ann Appl Biol. 1939;

75. Chemometec. Cell Count Assay. Available from: https://chemometec.com/resources/cell-assays/cell-count-viability-assay/

76. Tarnowski BI, Spinale FG, Nicholson JH. DAPI as a useful stain for nuclear quantitation. Biotech Histochem. 1991;66(6):296–302.

77. Djojosubroto M, Bollotte F, Wirapati P, Radtke F, Stamenkovic I, Arsenijevic Y. Chromosomal number aberrations and transformation in adult mouse retinal stem cells in vitro. Investig Ophthalmol Vis Sci. 2009;50(12):5975–87.

78. Dirks WG. Online STR matching analysis. 2013; Available from: https://www.dsmz.de/fp/cgi-bin/str.html

79. Freshney RI. Database of misidentified cell lines. Int J Cancer. 2010;126(1):302.

80. McKinnon KM. Flow cytometry: an overview. HHS Public Access [Internet]. 2018;0. Available from: https://www.ncbi.nlm.nih.gov/pmc/articles/PMC5939936/

81. Abcam. Introduction to flow cytometry. 2020; Available from: https://www.abcam.com/protocols/introduction-to-flow-cytometry

82. Virgo PF, Gibbs GJ. Flow cytometry in clinical pathology. Ann Clin Biochem. 2012;49(1):17–28.

83. Podhorecka M, Skladanowski A, Bozko P. H2AX phosphorylation: Its role in DNA damage response and cancer therapy. J Nucleic Acids. 2010;2010.

84. Ji J, Zhang Y, Redon CE, Reinhold WC, Chen AP, Fogli LK, et al. Phosphorylated fraction of H2AX as a measurement for DNA damage in cancer cells and potential applications of a novel assay. PLoS One. 2017;12(2):1–18.

85. Biolegend. FITC Annexin V. 2020; Available from: https://www.biolegend.com/fr-lu/products/fitc-annexin-v-5161

86. Rieger AM, Nelson KL, Konowalchuk JD, Barreda DR. Modified annexin V/propidium iodide apoptosis assay for accurate assessment of cell death. J Vis Exp. 2011;(50):3–6.

87. Harada A, Matsuzaki K, Takeiri A, Mishima M. The predominant role of apoptosis in γH2AX formation induced by aneugens is useful for distinguishing aneugens from clastogens. Mutat Res - Genet Toxicol Environ Mutagen [Internet]. 2014;771:23–9. Available from: http://dx.doi.org/10.1016/j.mrgentox.2014.05.010

88. Rogakou EP, Nieves-Neira W, Boon C, Pommier Y, Bonner WM. Initiation of DNA fragmentation during apoptosis induces phosphorylation of H2AX histone at serine 139. J Biol Chem [Internet].

2000;275(13):9390–5. Available from: http://dx.doi.org/10.1074/jbc.275.13.9390

89. Chung LY, Tang SJ, Wu YC, Yang KC, Huang HJ, Sun GH, et al. Platinum-based combination chemotherapy triggers cancer cell death through induction of BNIP3 and ROS, but not autophagy. J Cell Mol Med. 2020;24(2):1993–2003.

90. Torgovnick A, Schumacher B. DNA repair mechanisms in cancer development and therapy. Front Genet. 2015;6(APR):1–15.

91. Wang D, Lippard SJ. Cellular processing of platinum anticancer drugs. Nat Rev Drug Discov. 2005;4(4):307–20.

92. Martin LP, Hamilton TC, Schilder RJ. Platinum resistance: The role of DNA repair pathways. Clin Cancer Res. 2008;14(5):1291–5.

93. Edelbrock MA, Kaliyaperumal S, Williams KJ. Structural, molecular and cellular functions of MSH2 and MSH6 during DNA mismatch repair, damage signaling and other noncanonical activities. Mutat Res - Fundam Mol Mech Mutagen [Internet]. 2013;743–744:53–66. Available from: http://dx.doi.org/10.1016/j.mrfmmm.2012.12.008

94. Chen B, Zhong D, Monteiro A. Comparative genomics and evolution of the HSP90 family of genes across all kingdoms of organisms. BMC Genomics. 2006;7:1–19.

95. M F, Heltai S, Zocchi M, Rugarli C. Unusual expression and localization of heat-shock proteins in human tumor cells. Int J Cancer. 1992;

96. Lamboy-Caraballo R, Ortiz-Sanchez C, Acevedo-Santiago A, Matta J, Monteiro ANA, Armaiz-Pena GN. Norepinephrine-induced DNA damage in ovarian cancer cells. Int J Mol Sci. 2020;21(6).

97. Olive PL, Banàth JP. Kinetics of H2AX phosphorylation after exposure to cisplatin. Cytom Part B - Clin Cytom. 2009;76(2):79–90.

98. Derenzini E, Agostinelli C, Imbrogno E, Iacobucci I, Casadei B, Brighenti E, et al. Constitutive activation of the DNA damage response pathway as a novel therapeutic target in diffuse large B-cell lymphoma. Oncotarget. 2015;6(9):6553–69.

99. Velma V, Dasari SR, Tchounwou PB. Low doses of cisplatin induce gene alterations, cell cycle arrest, and apoptosis in human promyelocytic leukemia cells. Biomark Insights. 2016;11:113–21.

100. Shah MA, Schwartz GK. Cell cycle-mediated drug resistance: An emerging concept in cancer therapy. Clin Cancer Res. 2001;7(8):2168–81.

101. Sorenson C, Eastman A. Mechanism of cis-diamminedichloroplatinum(II)-induced cytotoxicity: role of G2 arrest and DNA double-strand breaks. Cancer Res [Internet]. 1988; Available from: https://pubmed.ncbi.nlm.nih.gov/3395999/

102. Ping W, Jiayue C, Jihong W, Yunhui G, Liangzi Z, Xia C. Cisplatin induces HepG2 cell cycle arrest through targeting specific long noncoding RNAs and the p53 signaling pathway. Spandidos Publ [Internet]. 2016; Available from: https://doi.org/10.3892/ol.2016.5288

103. Dolbeare F, Gratzner H, Pallavicini MG, Gray JW. Flow cytometric measurement of total DNA content and incorporated bromodeoxyuridine. Proc Natl Acad Sci U S A. 1983;80(18):5573–7.

104. Welschinger R, Bendall LJ. Temporal tracking of cell cycle progression using flow cytometry without the need for synchronization. J Vis Exp. 2015;2015(102):1–10.

105. Vignon C, Debeissat C, Georget MT, Bouscary D, Gyan E, Rosset P, et al. Flow Cytometric Quantification of All Phases of the Cell Cycle and Apoptosis in a Two-Color Fluorescence Plot. PLoS One. 2013;8(7):1–8.

106. Yuan CM, Douglas-Nikitin VK, Ahrens KP, Luchetta GR, Braylan RC, Yang L. DRAQ5-Based DNA Content Analysis of Hematolymphoid Cell Subpopulations Discriminated by Surface Antigens and Light Scatter Properties. Cytom Part B - Clin Cytom. 2004;58(1):47–52.

107. Abbott DR, Abbott RT, Jenson SD, Fillmore GC, Elenitoba Johnson KSJ, Lim MS. Apoptosis of t(14;18)-positive lymphoma cells by a Bcl-2 interacting small molecule. J Hematop. 2009;2(2):113–9.

108. Zhang Z, Xie Z, Sun G, Yang P, Li J, Yang H, et al. Reversing drug resistance of cisplatin by hsp90 inhibitors in human ovarian cancer cells. Int J Clin Exp Med. 2015;8(5):6687–701.

109. Mortensen ACL, Mohajershojai T, Hariri M, Pettersson M, Spiegelberg D. Overcoming Limitations of Cisplatin Therapy by Additional Treatment With the HSP90 Inhibitor Onalespib. Front Oncol. 2020;10(September).

110. Tung CL, Chiu HC, Jian YJ, Jian YT, Chen CY, Syu JJ, et al. Down-regulation of MSH2 expression by an Hsp90 inhibitor enhances pemetrexed-induced cytotoxicity in human non-small-cell lung cancer cells. Exp Cell Res [Internet]. 2014;322(2):345–54. Available from: http://dx.doi.org/10.1016/j.yexcr.2014.02.002

111. Goodspeed A, Jean A, Costello JC. A Whole-genome CRISPR Screen Identifies a Role of MSH2 in Cisplatin-mediated Cell Death in Muscle-invasive Bladder Cancer. Eur Urol [Internet]. 2019;75(2):242–50. Available from: https://doi.org/10.1016/j.eururo.2018.10.040

112. Yao Q, Weigel B, Kersey J. Synergism between etoposide and 17-AAG in leukemia cells: Critical roles for Hsp90, FLT3, topoisomerase II, Chk1, and Rad51. Clin Cancer Res. 2007;13(5):1591–600.

113. Roh JL, Kim EH, Park HB, Park JY. The Hsp90 inhibitor 17-(allylamino)-17-demethoxy geldanamycin increases cisplatin antitumor activity by inducing p53-mediated apoptosis in head and neck cancer. Cell Death Dis. 2013;4(12).

114. Schopf FH, Biebl MM, Buchner J. The HSP90 chaperone machinery. Nat Rev Mol Cell Biol [Internet]. 2017;18(6):345–60. Available from: http://dx.doi.org/10.1038/nrm.2017.20

115. Picard. HSP90 interactors [Internet]. 2022. Available from: https://www.picard.ch/downloads/Hsp90interactors.pdf

116. Medicine USNL of. The First-in-human Phase I Trial of PU-H71 in Patients With Advanced Malignancies [Internet]. Clinicaltrials.gov, U.S. National Library of Medicine. 2011. Available from: https://clinicaltrials.gov/ct2/show/study/NCT01393509

117. Selvakumaran M, Pisarcik DA, Bao R, Yeung AT, Hamilton TC. Enhanced cisplatin cytotoxicity by disturbing the nucleotide excision repair pathway in ovarian cancer cell lines. Cancer Res. 2003;63(6):1311–6.

118. Mirza-Aghazadeh-Attari M, Mohammadzadeh A, Yousefi B, Mihanfar A, Karimian A, Majidinia M. 53BP1: A key player of DNA damage response with critical functions in cancer. DNA Repair (Amst). 2019;73(October 2018):110–9.

119. Schultz LB, Chehab NH, Malikzay A, Halazonetis TD. p53 binding protein 1 (53BP1) is an early participant in the cellular response to DNA double-strand breaks. J Cell Biol. 2000;151(7):1381–90.

120. Durdik M, Kosik P, Gursky J, Vokalova L, Markova E, Belyaev I. Imaging flow cytometry as a sensitive tool to detect low-dose-induced DNA damage by analyzing 53BP1 and γH2AX foci in human lymphocytes. Cytom Part A. 2015;87(12):1070–8.

121. Croco E, Marchionni S, Bocchini M, Angeloni C, Stamato T, Stefanelli C, et al. DNA Damage Detection by 53BP1: Relationship to Species Longevity. Journals Gerontol - Ser A Biol Sci Med Sci. 2017;72(6):763–70.

122. Dhawan A, Bajpayee M, Parmar D. Comet assay: A reliable tool for the assessment of DNA damage in different models. Cell Biol Toxicol. 2009;25(1):5–32.

123. Wu J, Clingen PH, Spanswick VJ, Mellinas-Gomez M, Meyer T, Puzanov I, et al. γ-H2AX foci formation as a pharmacodynamic marker of DNA damage produced by DNA cross-linking agents: Results from 2 phase I clinical trials of SJG-136 (SG2000). Clin Cancer Res. 2013;19(3):721–30.

124. Mah LJ, El-Osta A, Karagiannis TC. γh2AX: A sensitive molecular marker of DNA damage and repair. Leukemia. 2010;24(4):679–86.

125. Lee Y, Wang Q, Shuryak I, Brenner DJ, Turner HC. Development of a high-throughput γ-H2AX assay based on imaging flow cytometry. Radiat Oncol. 2019;14(1):1–10.

126. Ivashkevich A, Redon CE, Nakamura AJ, Martin RF, Martin OA. use of the γ-H2AX assay to monitor DNA damage and repair in translational cancer research. NIH Public Access. 2012;

127. Quah BJC, Parish CR. The use of carboxyfluorescein diacetate succinimidyl ester (CFSE) to monitor lymphocyte proliferation. J Vis Exp. 2010;(44):4–7.